Title
Evaluation of the Gas Production Potential of Marine Hydrate Deposits in the Ulleung Basin of the Korean East Sea

Authors
Moridis, George J.
Reagan, Matthew T.
Kim, Se-Joon
et al.

Publication Date
2007-11-16

Evaluation of the Gas Production Potential of Marine Hydrate Deposits in the Ulleung Basin of the Korean East Sea

George J. Moridis, SPE, Matthew T. Reagan, SPE, Lawrence Berkeley National Laboratory, Se-Joon Kim, SPE, Korea Institute of Geoscience and Mineral Resources, Yongkoo Seol, and Keni Zhang, SPE, Lawrence Berkeley National Laboratory

Abstract
Although significant hydrate deposits are known to exist in the Ulleung Basin of the Korean East Sea, their survey and evaluation as a possible energy resource has not yet been completed. However, it is possible to develop preliminary estimates of their production potential based on the limited data that are currently available. These include the elevation and thickness of the Hydrate-Bearing Layer (HBL), the water depth, and the water temperature at the sea floor. Based on this information, we developed estimates of the local geothermal gradient that bracket its true value. Reasonable estimates of the initial pressure distribution in the HBL can be obtained because it follows closely the hydrostatic. Other critical information needs include the hydrate saturation, and the intrinsic permeabilities of the system formations. These are treated as variables, and sensitivity analysis provides an estimate of their effect on production.

Based on the geology of similar deposits, it is unlikely that Ulleung Basin accumulations belong to Class 1 (involving a HBL underlain by a mobile gas zone). If Class 4 (disperse, low saturation accumulations) deposits are involved, they are not likely to have production potential. The most likely scenarios include Class 2 (HBL underlain by a zone of mobile water) or Class 3 (involving only an HBL) accumulations.

Assuming nearly impermeable confining boundaries, this numerical study indicates that large production rates (several MMSCFD) are attainable from both Class 2 and Class 3 deposits using conventional technology. The sensitivity analysis demonstrates the dependence of production on the well design, the production rate, the intrinsic permeability of the HBL, the initial pressure, temperature and hydrate saturation, as well as on the thickness of the water zone (Class 2). The study also demonstrates that the presence of confining boundaries is indispensable for the commercially viable production of gas from these deposits.

Introduction
Background. Gas hydrates are solid crystalline compounds in which gas molecules (referred to as guests) occupy the lattices of ice crystal structures (called hosts). The hydration reaction of methane, the main gas ingredient of natural hydrates in geological systems, is described by the equation

$$CH_4 + N_H\, H_2O = CH_4{\bullet}N_H\, H_2O, \qquad (1)$$

where N_H is the hydration number that varies between 5.75 (for complete hydration) and 7.2[1], with an average value of N_H = 6. Such hydrates occur at locations in the permafrost and in deep ocean sediments where the necessary conditions of low T and high P exist for their formation and stability.

Current estimates of the size of the hydrocarbon resource trapped in hydrates vary widely[1,2,3] (ranging between 10^{15} to 10^{18} ST m^3), but the consensus is that it is vast, exceeding the total energy content of the known conventional fossil fuel resources. Even if only a fraction of the most conservative estimate of the resource is used as a basis of evaluation, its magnitude is sufficient large to command attention as a potential energy source[4,5]. This interest is further fueled by dwindling conventional hydrocarbon supplies, the rapidly expanding global demand for (and the corresponding rises in the cost of) energy, and the environmental desirability of CH_4 as a “clean” fuel. The emerging importance of hydrates as a potential gas resource was the impetus behind the proliferation of recent studies evaluating the technical and economic feasibility of gas production from hydrate deposits[5-11], and provided the motivation for this study.

The Ulleung Basin. This study focuses on the evaluation of the gas production potential from marine hydrate deposits in the Ulleung Basin of the Korean East Sea. The East Sea is a semi-closed marginal sea enclosed between the Eurasian continent and the Japanese Islands. The East Sea consists of three deep basins: the Ulleung, the Japan, and the Yamato (Figure 1).

The Ulleung Basin, located at the southwestern corner of the East Sea, is a bowl-shaped pull-apart basin formed by extension of continental crust during the Late Oligocene to Early Miocene and by compression at the Middle Miocene[12]. The west side of the basin is bounded by a narrow and steep sloped continental shelf, and the north side by a plateau with numerous ridges and troughs. The south and east sides of the basin are broad and gently sloped (Figure 1). The basin has a water depth of 1500-2300 m, and gradually deepens toward the north and the northeast[13]. The sediment thickness at the center of the basin is about 5 km[14], and increases to 10 km in its southern part[15]. Seismic stratigraphic analysis showed that the sediments in the Ulleung Basin consist of four distinctive subdivisions deposited in early Miocene to Quaternary[16].

Hydrates in the Ulleung Basin. Preliminary surveys conducted by the Korea Institute of Geoscience and Mineral Resources (KIGAM) between 2000 and 2004 suggest that there is a significant potential for gas hydrate occurrence in the Ulleung Basin[17]. The potential presence of gas hydrates in the basin has been suggested by several gas-related features identified by geophysical explorative analysis including (1) a shallow gas zone in the southwestern part of the basin, identified by high-resolution Chirp sub-bottom profiles and echo-sounding images, (2) gas-charged sediments and upward fluid migration, implied by acoustic turbidity and columnar structure of acoustic blanking in surveys of the area, (3) gas seepages on the continental slope, recognized by highly reflective, hyperbolic signals in the water column in echo-sounding images, (4) gas-related structures (pockmarks and domes) on the continental slope of the Ulleung Basin, detected by echo-sounding images[17].

Analysis of piston core samples recovered from the western Ulleung Basin[13] showed rapid sedimentation rates, high heat flow, and high total organic carbon and residual hydrocarbon gas, which suggest favorable conditions for the formation of natural gas hydrates in the region. Recently, KIGAM collected hydrate samples from shallow sediments from 7.8 m below the sea floor at a water depth of 2072 m. The sampling point was located in the center of the basin, 100 km south of the Ulleung Islands. Hydrates were found intermittently in the 6.5 m to 7.8 m interval below the sea floor, where a 2-m thick hydrate layer was found. The sample was 99% CH_4-hydrate intercalated in clayey sediments.

Based on the recent successful sampling and the aforementioned indications of hydrate presence in the Ulleung Basin, KIGAM selected five locations for deep drilling. Core retrieval to a depth of 200 m is planned at these locations. Data from these cores will be used to provide a first insight into the characteristics of the possible hydrate accumulations in this area, and may be used to evaluate the technical and economic feasibility of gas production from promising accumulations.

Objective and approach. The main objective of this study is to assess the production expectations from potential hydrate accumulations in the Ulleung Basin by means of numerical simulation. At this time, information on the properties of the hydrate-bearing formations at the drilling target sites (including initial conditions, lithology and hydrological properties of the host rock, reservoir stratigraphy, thickness, extent and boundaries of the hydrate zone, and the possible presence of underlying zones of mobile fluids) is either scant and/or not publicly available. Therefore, the parameters used in the reference cases of this study are reasonable estimates that are based on the properties of other marine hydrate deposits (on which more data are available), adjusted for the local geologic conditions. Because of the significant uncertainties, a large number of these parameters are treated as perturbation variables in the ensuing sensitivity analysis.

Because of the strong dependence of the gas production method on the geology of the hydrate-bearing systems[6-8] and the paucity of data on the subject, it is not possible to focus on a particular type of hydrate accumulation and a corresponding production method. Therefore, this study encompasses the most likely types of hydrate deposits and addresses the various factors and issues that may affect production from them.

In evaluating the production potential of likely hydrate deposits in the Ulleung Basin, we used two criteria, an absolute criterion and a relative criterion. To satisfy the absolute criterion, a large production potential must be demonstrated, as quantified by an early large gas production rate Q_P (> 2 ST m^3/s = 6 MMSCFD), a large cumulative gas production volume V_P, and a large average gas production rate Q_{avg} (> 1 ST m^3/s = 3 MMSCFD) over the duration of the study (typically the 30-year life expectation a commercial gas well). The relative criterion is satisfied when the water-to-gas ratio $R_{WGC} = M_W/V_P$ is low, indicating a small cumulative mass of produced water M_W (an inevitable result of the hydrate dissociation) relative to V_P, thus reducing the significant energy requirements for the water lift and the corresponding environmental concerns associated with its disposal.

Additionally, we monitored the salinity of the produced water because of its cost, energy demand, and environmental implications. Because water from dissociation is fresh, its disposal at the sea surface may not face significant regulatory challenges (especially in deep seas), but lifting large water volumes to the surface can burden gas production with additional costs, energy usage, and environmental loading. Considerable cost savings and environmental benefits may be possible if the produced water can be disposed of near the ocean floor, but such releases may have to meet environmental regulations designed to protect chemosynthetic communities (as well as other flora and fauna) at the ocean floor that may not be able to survive a significant change in salinity.

System Description and Production Strategies

Classification of hydrate deposits. Natural hydrate accumulations are divided into three main classes.[6-8] Class 1 accumulations are composed of two layers: the Hydrate-Bearing Layer (hereafter referred to as HBL), and an underlying two-phase fluid zone containing free (mobile) gas and liquid water. Class 2 deposits comprise a HBL overlying a zone of mobile water (hereafter referred to as WZ). Class 3 accumulations involve a HBL without an underlying zone of mobile fluids. Class 4 deposits[9] are almost exclusively marine accumulations, and involve disperse, low-saturation hydrate occurrences that lack confining geologic strata and are commonly encountered in marine environments.

Types of hydrate deposits in the Ulleung Basin. As indicated early, knowledge on the state and properties of potential hydrate deposits in the Ulleung basis is very limited. To reduce the large number of possible scenarios (of geology and the corresponding production strategies) to manageable levels, we excluded from the study entire classes of hydrate deposits based on their (a) general production potential, and (b) probability of occurrence.

Although Class 4 deposits are certain to occur in the Ulleung Basin (as the piston core samples have indicated[13]), they were removed early from consideration. Earlier work[9] has shown convincingly that such deposits are not promising production targets under any combination of system properties, initial conditions, and operational parameters.

There is no confirmed occurrence of Class 1 deposits at the site, but indications of (a) a shallow gas zone in the southwestern part of the basin, and (b) of gas-charged sediments and upward fluid migration[17] make their existence a possibility. However, the likelihood of the existence of a significant number of such deposits (and/or of large size) is rather limited. This is because such incidence would require the confluence of relatively unique geologic conditions, with the reservoirs cross cutting the base of the gas hydrate stability field (i.e., the location above which hydrates are stable because of thermodynamically favorable pressure P and temperature T conditions). Additionally, the lithology of the Ulleung Basin indicates dominance of fine sands interlayered with silts and clays, a regime that is not conducive to significant free gas and/or hydrate accumulations. Although such deposits can be very productive[6], their expected rarity and the very large computational resources needed for their analysis[6] did not make them attractive subjects for this study.

Thus, we focused on the hydrate deposit classes that are most likely to occur at the site, Classes 2 and 3, which are also the two most common classes of hydrate accumulations in both the permafrost and in the oceans. In these two classes the bottom of the hydrate stability zone occurs below the bottom of the hydrate interval, i.e., the entire HBL is within the hydrate stability zone. Previous studies of gas production from deeper and significantly warmer deposits[7,8] indicated production rates as high as Q_P = 5.48 ST m^3/s (= 16.72 MMSCFD) and Q_P = 5 ST m^3/s of CH_4 (15 MMSCFD) from Class 2 and Class 3 deposits, respectively. Although sensitivity analyses[7,8] indicated that gas production generally declines in shallower, colder and less permeable formations (such as the ones in the Ulleung Basin), the limited body of previous work on the subject do not allow extrapolation of past results, especially when the issue is complicated by the larger HBL thickness at the site and the use of specialized well designs (discussed below).

Note that the reference cases in this study involve Class 2 and Class 3 accumulations that are confined between nearly impermeable overburdens and underburdens. Without such strata, gas production can be disappointing because flow through the boundaries limits the effectiveness of depressurization and leads to large production volumes of undesirable water[19]. While a confining underburden is highly desirable in production from Class 2 deposits, a near-impermeable overburden is critically important to both classes because of large gas accumulations above the hydrate body (a feature typical of gas production from hydrates that follows the evolution of an upper receding dissociating interface)[7,8]. Lack of a confining overburden could lead to gas loss though the overburden toward the surface.

Dissociation methods. Gas can be produced from hydrates by inducing dissociation using one of the three main dissociation methods[18] (or combinations thereof): depressurization, thermal stimulation, and the use of inhibitors.

Earlier studies[6-9] appear to indicate that depressurization is the most promising dissociation method (and possibly the only practical option) in the majority of hydrate deposits because of its simplicity, its technical and economic effectiveness, the fast response of hydrates to the rapidly propagating pressure wave, the near-incompressibility of water (which expands the volume over which depressurization is sensed by the HBL), and the large heat capacity of water. The latter plays a significant role in providing part of the heat needed to support the strongly endothermic dissociation reaction as warmer water flows from the outer reaches of the formation toward the well. Numerical studies have shown that the other dissociation methods enhance gas production when used in conjunction with depressurization[7,8], but tend to be ineffective when used as the main dissociation strategies[8].

Method of production from Class 2 deposits. Gas is produced from Class 2 deposits by removing reservoir fluids from a well operating at a constant mass rate Q_M[7]. The presence of the WZ allows depressurization of the deposit even when the effective permeability k_{eff} of the HBL is very small because of a low intrinsic permeability k and/or a high hydrate saturation S_H. Flow blockage caused by the formation of secondary hydrate or ice can be removed by the short-term application of thermal stimulation, involving the injection of warm water[7-8].

Method of production from Class 3 deposits. Constant-pressure production is the recommended depressurization method for gas production from Class 3 deposits[8] because (a) it is applicable to a wide range of formation permeabilities, (b) is uniquely suited to allow continuous rate increases to match increasing permeability (the result of the dissociation-caused reduction in S_H), and (c) may be the only reasonable alternative when S_H is high.

Well designs in Class 2 deposits. The well system used in gas production from the Class 2 deposits involved different well configurations at different times during the production period. It is a modification of the well design used in a deeper, warmer reservoir described by Moridis and Reagan[7]. The heated wellbore used during the initial production phase in that problem turned out to be problematic in the shallower, colder deposits of the Ulleung Basin because the released gas moved radially deeper into the HBL, increasing the pressure and resulting in additional hydrate formation that was further promoted by the reduction in the water salinity (because of dilution by the released fresh water). The result was the development of a high-S_H and practically impermeable secondary hydrate barrier surrounding the wellbore that sealed the hydrate body and prevented communication with the evolving upper dissociating interface.

Phase 1. In the well design used during the initial phase of production from Class 2 deposits in the Ulleung Basin, the perforated interval was unheated and extended through the entire HBL thickness well into the WZ (Figure 2). This design has significant advantages[7]: the active production interval becomes progressively larger as hydrate dissociation advances, k_{eff} in the HBL next to the well increases continuously, and milder pressure drops and lower gas velocities result (thus reducing cooling and the potential for secondary hydrate formation). Additionally, this well design promotes the evolution of a cylindrical interface of hydrate dissociation around the well, providing access to both the lower and the upper horizontal dissociation interfaces at the bottom and top of the hydrate body.

Phase 2. An earlier study had indicated that this design caused significant dissociation around the well and yielded the largest production rates, but when used over long periods, it could result in conditions conducive to extensive secondary hydrate formation. This potential problem was avoided by moving into the well design of Phase 2 at the first sign of secondary hydrate formation around the well. This involved warm water injection through the upper part of the wellbore (Figure 3), and is the same as in the *Moridis and Reagan*[7] study. The unique feature of this well design is that it prevents the formation of secondary hydrate around the wellbore[7]. This results in maximum gas release and production by providing unimpeded access to the three interfaces (i.e., the cylindrical, the upper and the lower horizontal ones).

Phase 3. The well may be further modified at a later stage (usually when a fraction of the original hydrate remains) when there is significant gas accumulation at the top of the reservoir. Despite high pressures and large volumes, this gas cannot be recovered by using a conventional well perforated at the top of the formation because, after an initial short, high-rate, production period (lasting from hours to weeks), the well is blocked by secondary hydrate and ice. The problem is alleviated by modifying the well according to the design shown in Figure 4, which involves alternating thin zones (about 1 m) of gas production and warm water injection. The warm water is injected at a low rate (< 1 kg/s) at a relatively low temperature (the reservoir is already cold because this well phase begins operating at a time corresponding to an advanced stage of dissociation), and either prevents the formation of secondary hydrate or ice through mixing with the incoming fluid stream, or destroys pre-existing hydrate and ice blockages by thermal stimulation.

Well designs in Class 3 deposits. This well design is quite simple, and involves a perforated interval that covers the entire thickness of the HBL. A significant advantage of constant-*P* production is the elimination of the possibility of ice formation (with its detrimental effects on permeability and Q_P) through the selection of an appropriate well pressure P_w. This is ensured by selecting a $P_w > P_Q$ (= *P* at the quadruple point).

The Numerical Models and Simulation Approach

The numerical simulation code. The numerical studies in this paper were conducted using the TOUGH+HYDRATE simulator, the successor to the earlier TOUGH-Fx/HYDRATE model.[20] This code can model the non-isothermal hydration reaction, phase behavior, and flow of fluids and heat under conditions typical of natural CH_4-hydrate deposits in complex geologic media. It includes both an equilibrium and a kinetic model[21,22] of hydrate formation and dissociation. The model accounts for heat and up to four mass components (i.e., water, CH_4, hydrate, and water-soluble inhibitors such as salts or alcohols) that are partitioned among four possible phases: gas, aqueous liquid, ice, and hydrate. A total of 15 states (phase combinations) can be described by the code, which can handle any combination of hydrate dissociation mechanisms and can describe the phase changes and steep solution surfaces that are typical of hydrate problems. Because of the very large computational requirements of this type of problems[7,8], both the serial and the parallel (MPI) versions of the code were used in the simulations.

System geometry. The geologic system in this study corresponds to a location at the Ulleung basin where the sea floor is at an elevation of z = -1800 m. The HBL is 50 m thick, and both the Class 2 and Class 3 systems are overlain by a nearly impermeable, 180 m-thick overburden. The Class 2 system is underlain by a by a 15 m-thick WZ bounded at the bottom by a 15 m-thick impermeable underburden, while the Class 3 deposit is underlain by only a 30 m-thick impermeable underburden.

The geometry and configuration of the Class 2 system are shown in Figure 5. Based on earlier studies[6-8], a 30 m overburden was considered in the simulations because this was sufficient to allow accurate heat exchange with the hydrate deposit during a 30-yr long production period (i.e., the standard life cycle of a well). Similarly, inclusion of the WZ and the 15-thick underburden (Class 2) and the single, 30 m-thick impermeable underburden (Class 3) was sufficient to provide accurate estimates of heat transfer in each case.

The well at the center of this cylindrical hydrate deposit (Figure 5) had a radius r_w = 0.1 m. A no-flow boundary (of fluids and heat) was applied at the reservoir at radius r_{max} = 567.5 m. This corresponds to a well spacing of about 100 ha (= 250 acres), and the no-flow boundary assumed the presence of other wells on the same spacing pattern.

Domain discretization and media properties. The same grid and media properties were used in both the Class 2 and Class 3 simulations. In the absence of field data from the site, reasonable estimates of the media properties (considered representative of media similar to those of the general Ulleung Basin lithology) were assumed (Table 1). The cylindrical domain was discretized into 103 x 142 = 14,626 gridblocks in (r,z), of which 14,280 were active (the remaining being boundary cells). The uppermost and lowermost layers corresponded to constant *T*. Because the vicinity of the wellbore (especially the r < 20 m zone) had been shown to be critically important to production[7,8], we used a very fine discretization along the *r* direction in this region.

The HBL was subdivided into segments of $\Delta z \leq 0.50$ m each along the *z*-direction. Such a fine discretization of is important (and possibly necessary) for accurate predictions[6,7], but a coarser discretization along the *z* axis is permissible in the WZ[7]. This high degree of refinement provided the level of detail needed near the wellbore and in the entire hydrate-bearing zone. Assuming an equilibrium reaction of hydrate dissociation[22], the grid resulted in 57,120 coupled equations that were solved simultaneously.

Well description. The importance of the near-well region dictated the physical representation of the wellbore in both the Class 2 and Class 3 studies. To avoid the theoretically correct but computationally intensive solution of the Navier-Stokes equation, we approximated wellbore flow by Darcian flow through a pseudo-porous medium describing the interior of the well. Earlier studies had shown the validity of this approximation[7]. This pseudo- medium had a $\phi = 1$, a very high $k = 10^{-9}$-10^{-8} m^2 (=1,000-10,000 Darcies), a capillary pressure $P_c = 0$, a relative permeability that was a linear function of the phase saturations in the wellbore, and a low (but nonzero) irreducible gas saturation $S_{irG} = 0.005$ (necessary to allow the emergence of a free gas phase in the well).

Initial conditions. We determined the initial conditions in the reservoir by following the initialization process described by *Moridis et al*.[6-8] Knowing (a) the elevation at the base of the HBL, and (b) assuming that the pressures in the oceanic subsurface follow the hydrostatic distribution (a hypothesis supported by field observations from other hydrate accumulations[23]), we determined the pressure P_B (at z = -2030 m, see Figure 5) using a *P*- and *T*-adjusted saline water density typical of ocean water (1035 kg/m^3 at atmospheric pressure).

The hydrate *P-T* equilibrium curve was then used to provide the upper limit of T_B at that location (i.e., the equilibrium *T*). In terms of production, the most desirable initial conditions then involve a T_B that is slightly lower than the equilibrium *T* because such a system is easy to destabilize. For the known *T* at the mudline (= 1.7 ^oC), the local geothermal gradient was computed as dT/dz = 0.0509 K/m, and was used to determine the initial T at the top and bottom boundaries, from which the remaining information on the temperature profile was obtained by means of a short simulation.

Production from the Reference Case of a Marine Class 2 Deposit in the Ulleung Basin

The reference case. The properties and conditions pertaining to the reference case are listed in Table 1. Because earlier studies[7] had shown that the production performance of Class 2 deposits improves with an increasing Q_M, the initial mass rate of fluid production from the well was set at a high level, i.e., Q_{M0} = 36.8 kg/s (= 20,000 BPD of water). Then the resulting gas and aqueous phase production rates (Q_P and Q_W, respectively) were determined from the phase mobilities. The pressure in the well was continuously monitored, and was immediately adjusted when *cavitation* occurred[7,8]. Cavitation is characterized by a rapid pressure drop to levels below atmospheric, and can result from either (a) flow blockage because of the formation of secondary hydrate and/or ice, or (b) the increasing participation of gas in the production stream. The latter is caused by increasing volumes of low-density gas replacing the denser water, reaching a point where the system effective permeability is incapable of supplying the well with the prescribed Q_M. The continuing pressure drop in the deposit (which further reduces the gas density and overwhelms the opposite effects of the lower temperatures that accompany hydrate dissociation) accentuates the problem.

When increasing gas production is the cause, reducing Q_M can alleviate the cavitation. Note that a reduction in Q_M does not necessarily lead to a decline in Q_V because gas production can return to (and often exceed) the rate prior to cavitation. When cavitation is caused by flow blockage, then reduction in Q_M provides very short-term benefits, and the problem can only be alleviated by removing the underlying cause, e.g., by injection warm water that destroys the secondary hydrate and/or ice accumulation.

Gas and water production. Figure 6 shows the evolution of the volumetric rates (a) Q_R of CH_4 released from hydrates in the entire simulated domain, and (b) Q_P of CH_4 production at the well. The jagged (see-saw) appearance of the two curves is caused by frequent Q_M reductions in response to cavitation, and confirms the earlier comment that a reduction in Q_M is often followed by an increase in Q_P. Q_R initially increases rapidly as the depressurization disturbance propagates along the lower interface (because of the near-incompressibility of water) and induces dissociation. The Q_M adjustments are clearly evident in the evolution of Q_W (which initially represents the bulk of the produced fluids) in Figure 7, which shows a continuous step-type decline. Consistent with previous studies[7,8], the common pattern of hydrate behavior applies here, with (a) Q_P, Q_R increasing monotonically, and (b) Q_W decreasing monotonically during each cycle, i.e., the period between two successive cavitation effects.

A local maximum of Q_R = 3.45 ST m^3/s (= 10.53 MMSCFD) is reached before a decline begins. This is attributed to a combination of (a) a decrease in the driving force of depressurization as the pressure differential between the well and the HBL is reduced, (b) gas accumulation in the deposit, as the released gas at the advancing dissociation fronts cannot yet be produced at the well because $S_A < S_{irA}$, and (c) the resulting lower T, which further slows dissociation. Meanwhile, after about 300 days of initial, practically constant, production fueled mainly by the release of dissolved gas[7], Q_P increases monotonically.

The rapid Q_R decline at about t = 1000 days is due to well *choking* and cavitation caused by the emergence of secondary hydrate and ice near the well. At that time, the well configuration is switched to Phase 2 (Figure 4), which temporarily results in a Q_R decline because of the change in the location and size of the production interval. Q_P also declines, as the new production interval promotes water (rather than gas) production. Warm ocean water begins to be injected at a rate of Q_I = 1 kg/s (about 530 BPD) and a specific enthalpy $H_W = 2.2\text{x}10^5$ J/kg (corresponding to a temperature of about 55 ^oC at the injection pressure). Q_R is quickly restored to pre-choking levels, but does not attain the maximum level observed during Phase 1 because the injected warm water adversely affects gas production. Thus, the maximum Q_R in Phase 2 is 2.70 ST m^3/s (= 8.24 MMSCFD), with Q_R varying within a narrow range. The different well design is the reason for this Q_R behavior, which is distinctively different from that of the deeper, warmer system studied by *Moridis and Reagan*[7]. In Phase 2, Q_P increases initially to reach Q_P = 3.07 ST m^3/s (= 9.37 MMSCFD). It then begins to decline as Q_R declines, and $Q_P > Q_R$ for the remainder of the study (indicating a dissociation deficit, and production supported by gas stored in the reservoir).

The introduction of the Phase 3 well design at t = 3,400 days does not appear to have any benefits, as the Q_R decline continues unabated. This is in contrast to the Q_R behavior in the enhanced recovery phase in Case C of the *Moridis and Reagan*[7] study, which showed significant production increases. The differences in performance become even more pronounced at t = 3,575 days, when gas production cannot be maintained because of very low temperatures (< 0 ^oC) and insufficient gas releases. Although gas release from hydrate dissociation continues ($Q_R > 0$), it is at a very low level, $Q_R < Q_P$. After evaluating several alternatives, a plausible option appears to be the cessation of production operations ($Q_M = 0$) for a certain period (1 year) to allow the thermal recovery of the system by heat influxes fueled by the geothermal gradient. Production was then resumed at t = 3,940 days, but it was again short-lived as T returned to its previous levels within 230 days, needing another rest period before it could resume. If continuation of production past this point is desired, such cycles of repose and production appear to be a possibility. However, it must be stated that the matter has not been fully researched, and other options may offer better performance.

Figure 6 also shows the evolution of the average gas production $Q_{avg} = V_P/t$. This quantity provides an additional criterion for the determination of the point when production becomes uneconomical (in addition to the Q_P magnitude), i.e., it describes the average production up to any time t. Thus, the maximum Q_{avg} (= 2.00 ST m^3/s = 6 MMSCFD) is observed at t = 4186 days, and afterwards begins to decline during the long periods of thermal recovery.

Figure 8 shows the cumulative volumes (a) V_R of CH_4 released from hydrates in the entire simulated domain, and (b)

V_P of produced CH_4 at the well. At the end of this simulation (t = 4186), the hydrate is far from exhausted (about 50% still remains), and $V_P > 0.8\ V_R$. During this period, a total of V_P = 6.67x10^8 ST m^3 (= 2.35x10^{10} ST ft^3) of CH_4 were produced.

The implication from these observations is that while large volumes of CH_4 can be produced from Class 2 deposits in the Ulleung Basin, production does not continue uninterrupted until the exhaustion of hydrate, but can cease when the HBL temperature drops to low levels. This is starkly different from the behavior of deeper, warmer Class 2 deposits[7]. A possible mechanism to alleviate the problem is production cessation to allow thermal recovery of the HBL. Given the fact that a large fraction of the original hydrate (about 50%) remains in the reservoir, it is possible that such an approach (employing the geothermal gradient to replenish the depleted heat reservoir in the HBL) is a viable option. However, no definitive conclusions can be reached.

Spatial distributions of S_H and S_G. The white lines in all of the figures that describe the spatial distribution of reservoir properties and conditions in Figures 9 to12 indicate the initial position of the base of the HBL, while the top of the HBL co-incides with the z = –30 m datum. Comparison of the hydrate distribution to the initial HBL extent provides a measure of the magnitude of dissociation of the hydrate.

Figures 9 and 10 show the evolution of the S_H and S_G distributions over time in the deposit near the wellbore (r < 100 m). The dissociation pattern is similar to that in the *Moridis and Reagan*[7] study, These include (i) hydrate dissociation proceeding initially along the lower hydrate interface, being more pronounced (as expected) close to the well, (ii) the evolution of a cylindrical dissociation interface around the well, (iii) the evolution of the upper dissociation interface, and (iv) the accumulation of gas between the receding upper hydrate interface and the base of the overburden. Of those, (i), (iii) and (iv) are universal features of depressurization-induced hydrate dissociation[6-8], and (iii) and (iv) are a result of continuing depressurization and heat flows from the upper boundary (where there is an inversion of the geothermal gradient because of dissociation-induced cooling in the HBL).

The absence of any secondary hydrate in Figure 9 is remarkable. The well choking event at t = 1,000 days was of limited duration, and the flow obstruction was eliminated within a few days after the switch to the Phase 2 well design. The uninterrupted flow paths contribute to the smooth distribution patterns observed in Figure 9. The several cavitation events that are evident at the end of each production cycle in Figure 6 (denoted by the subsequent drops in Q_P and Q_R, as dictated by the need to reduce the Q_M rate for reasons already discussed) are not caused by secondary hydrate formation but by the continuous replacement of the denser water by the lower-density gas in the production stream. The S_H distributions in Figure 9 validate this hypothesis that this design prevents secondary hydrate formation, and allowed unhindered communication between the dissociation interfaces and the well. The S_H distribution in Figure 9f shows the significant destruction of hydrate at the end of t = 4,137 days.

The S_G distributions in Figure 10 indicate accumulation in the hydrate-free zone between the base of the overburden and the receding upper hydrate interface, leading to the highest S_G observed in the deposit. The S_G at this location increases with time, but significant cooling at advanced times during production prevents the recovery of this gas (Figure 6). The reason for this accumulation is the continuing dissociation along the upper interface, in addition to the rising of the gas released elsewhere in the deposit due to buoyancy. The emergence of the upper dissociation interface and the corresponding gas accumulation at the top of the HBL underlines the necessity for upper permeability barriers if gas production from hydrates is to become possible. Absence of such barriers will inevitably lead to gas losses through the permeable overburden toward the surface, with undesirable consequences if such releases cannot be contained.

Dissociation and gas release along the bottom of the hydrate interval continue, resulting in gradually increasing S_G and the development of a modest gas bank at that location (Figures 10b and beyond). However, S_G is significantly lower than that at the top of the HBL because continuous flow to the well and buoyancy-driven rise through the hydrate body (Figures 9 and 10) prevents gas accumulation. Note the S_G reduction along the bottom of the domain (especially evident in Figures 10e and 10f), which is caused by the accumulation of draining water released from dissociation.

Spatial distributions of *T*. The T distribution in Figure 11 indicates continuous (and uniform) cooling as dissociation and production proceed, and confirms expectations. The warm water injection during Phase 2 and 3 of the well operation is clearly depicted by the occurrence, spatial distribution and shapes of the temperature anomalies near the wellbore. The rising deeper water (moving toward the well in early in the production period (Figures 11a and 11b) can be easily identified, as can regions of intense hydrate dissociation as the locations where significant T drops are observed.

Spatial distributions of X_S. The distribution of the salt concentration (expressed as the mass fraction of salt X_S in the aqueous phase) in Figure 12 shows the dilution effect of dissociation on salinity, and is analogous to the observations from the study of deeper, warmer deposits[7]. Because salts cannot be included in the hydrate crystals, fresh water is released upon dissociation and reduces the water salinity. Thus, the locations of intense dissociation activity can be identified as the loci of low salinity. This maximum X_S reduction is observed near the top of the HBL because of continuing removal (through production), dilution, and drainage of the native saline water, in addition to limited replenishment of salinity from native water flowing from the nearly impermeable boundaries. Because of proximity to the underlying WZ, the salinity reduction is less pronounced at the lower dissociating interface. The signature of the injected saline water (part of the well configurations in Phases 1 and 2) can also be easily discerned.

Sensitivity Analysis of Production From Class 2 Deposits in the Ulleung Basin

In these deposits, we investigated the sensitivity of gas production to the following conditions and parameters:

(a) The initial hydrate saturation S_{H0}

(b) The intrinsic permeability k
(c) The stability of the hydrate deposit, as quantified by its temperature T and its deviation from the equilibrium temperature at the prevailing pressure
(d) The initial mass production rate Q_{M0}
(e) The well spacing L_W

The results of these analyses are presented in Figures 13 through 15.

Sensitivity to S_{H0}. Figure 13a shows the dependence of Q_P on S_{H0}. Under the conditions of the Ulleung basin, a lower S_{H0} leads to a higher Q_P because the advantage of the higher initial effective permeability (and, consequently, a faster depressurization and hydrate dissociation) persists over a long time because of the large fraction of the hydrate remaining in the reservoir at the end of the production periods we investigated. Thus, the reduction of the resource does not reach levels of "leanness" that would result in rapid Q_P decline. This is the case in the deeper warmer oceanic deposits in the *Moridis and Reagan*[7] study, which exhibit an inversion of the relationship after an initial period.

This behavior of potential Class 2 deposits in the Ulleung Basin is also illustrated by the evolution of the cumulative volume of produced gas V_P, which is highest for the lowest S_{H0} = 0.30 and lowest in the reference case, in which S_{H0} = 0.65 (Figure 14a). In absolute terms, large gas volumes V_P are produced before the repository cooling leads to the need for thermal recovery. The cumulative mass of produced water M_W also increases with a decreasing S_{H0} (as expected, given the correspondingly larger S_A), but the effect is much weaker than that of the Q_P and V_P dependence on S_{H0}. This leads to the water-to-gas ratio R_{WGC} of Figure 15a, which is initially favored by a high S_{H0} because of the lower permeability of the remaining aqueous phase. However, this relationship is later inverted, as considerably more gas is produced by the low S_{H0} systems, leading to favorable water-to-gas ratio. Figure 15a shows that the R_{WGC} performance is not strictly a function of S_{H0}, but varies significantly over time, with the best long-term R_{WGC} performance corresponding to the case of S_{H0} = 0.30. Thus, conclusions about the system behavior can only be considered as coupled functions of the system parameters and the time frame of production. It is obvious that the initial hydrate saturation has one of the strongest effects on the gas production potential of these Class 2 deposits in terms of both the absolute and the relative evaluation criteria.

The effect of S_{H0} on the salinity in the produced water X_P is demonstrated in Figure 15b. These results indicate that the well design we employed in this study results in mild salinity changes not only for varying S_{H0}, but also for any of the perturbation parameters considered here. This is accomplished by providing access to the saline WZ, resulting in salinity reductions of less than 15% from its original level of 0.035 over the production period. It is possible that biota near the ocean floor may not be significantly affected by such a mild change in salinity. Even in cases of increased sensitivity, it is rather easy to release water of acceptable salinity after mixing with appropriate quantities of ocean water. The lower water production from the S_{H0} = 0.65 case results in higher X_S. The S_{H0} = 0.30 case shows less of an effect on X_S because the more limited hydrate mass has a less pronounced effect on the larger mass of saline water mass than in the S_{H0} = 0.50 case. Note that X_S may be a necessary, but not sufficient, evaluation criterion because of the potential importance of other chemical species, such as oxygen, in the released waters.

Sensitivity to k. By reducing k to $2.5\text{x}10^{-13}$ m^2 (= 250 mD, 50% of its reference value), we observe deterioration in performance, as evaluated using the absolute criterion and the results in Figures 13a and 14a. The effect of k on Q_P and V_P is superlinear, corresponding to a production reduction that exceeds the reduction of k. While water production is also reduced (see M_W in Figure 14b), its positive effect is negated by the gas production reduction. Note that the results in Figure 13b and 14 incorporate rate reductions that are automatically introduced when cavitation begins to occur. In other words, the results of all the sensitivity analyses reflect performance while maintaining production at its maximum possible level.

Performance against the relative criterion of R_{WGC} (Figure 15a) also deteriorates, after initially being similar to that of the reference case (but corresponding to far less gas). The obvious conclusion is that a declining k has a pronounced adverse effect on the gas production potential. As expected, the evolution of X_S shows a milder decline than the reference case.

Sensitivity to T. Figure 13b shows the dependence of Q_P on the hydrate stability, as quantified by the system temperature T (in this case reduced by about 2.5 ^{o}C by reducing the geothermal gradient to dT/dz = 0.04 K/m), while keeping P equal to the reference case. The colder and more stable system results in a markedly (and consistently) lower Q_P. For the same reason, the corresponding V_P in Figure 14a is substantially lower than that in the reference case, while M_W in Figure 14b is also lower because of a lower k_{eff} in the presence of a hydrate that resists dissociation. The resulting R_{WGC} in Figure 15a shows a very strong dependence on T (on a par with that to k), indicating larger water production in more stable systems (as expected), and demonstrates the importance of temperature as a selection criterion of a hydrate deposit as a production target. For a given pressure, the desirability of such deposits increases with T and with the proximity of T to the equilibrium temperature. The effect of T on X_S (Figure 15b) is similar to that for a lower k, and shows a milder decline than the reference case.

Sensitivity to Q_{M0}. By reducing Q_{M0} to $0.5Q_{M0,ref}$, where $Q_{M0,ref}$ is the Q_{M0} in the reference case, we observe deterioration in performance, as evaluated using the absolute criterion and the results in Figures 13b and 14a. The effect of Q_{M0} on Q_P and V_P is sublinear, corresponding to production reduction that is substantially less than the reduction in Q_{M0}. This sublinear decline is attributed to lower dissociation rates (resulting in higher temperatures) and the continuing influx of heat through the constant-T boundaries. Water production is also reduced (see M_W in Figure 14b), but the impact on both the absolute and the relative criteria are outweighed by the reduction in gas production. Thus, the relative performance (as quantified by R_{WGC} in Figure 15a) is among the worst both at early and later times. This result confirms the validity of an earlier study[7] that concluded that gas production (as measured by both the absolute and relative criteria) improves with Q_{M0}, and the highest possible production rate should be imposed at the well for optimal results. As expected, because of reduced production and dissociation, the released fresh water is also reduced, leading to the very mild decline of X_S in Figure 15b.

Sensitivity to L_W. Increasing the well spacing from L_W = 100 ha (=250 acres) to L_W = 380 ha (=960 acres) required a new grid with 125x142 = 17,750 cells in (*r,z*). The results showed one of the worst performances, as evaluated using the absolute criterion and the results in Figures 13b and 14a. The effect of L_W on Q_P and V_P is sublinear, but the larger system generates the lowest Q_P and V_P and also the highest M_W (see Figures 13b and 14). The corresponding R_{WGC} (Figure 15a) has the highest value (and consequently, the worst relative performance) of all other perturbation parameters, These results are a clear indication of the strong dependence of production on well spacing, and of the need to use that the smallest possible L_W (as limited by economic and technical considerations) for optimal production from Class 2 deposits in the Ulleung Basin. As expected, because of a much larger initial amount of water in the WZ in this case, the reduction in X_S in Figure 15b is the lowest.

Production from the Reference Case of a Marine Class 3 Deposit in the Ulleung Basin

The reference case. The properties and conditions pertaining to the reference case are listed in Table 1. This simple well design employs a constant bottomhole pressure, and is described by an internal boundary located in a gridblock above the uppermost gridblock in the well subdomain. By imposing a constant bottomhole pressure P_w and a realistic (though unimportant) constant temperature T_w at this internal boundary, the correct constant-*P* condition was applied to the well while avoiding any non-physical temperature distributions in the well itself (the large advective flows into the uppermost gridblock from its immediate neighbor eliminated any potential reverse heat transfer effects that could have resulted from an incorrect T_w). The initial bottomhole constant P_w = 2.8 MPa > P_Q, thus eliminating the possibility of ice formation and the corresponding potentially adverse effect on k_{eff}. This production method is based on a very simple well design that involves conventional technology and poses no particular technical challenges.

Evolution of gas and water releases. Figure 16 shows the evolution of the volumetric rates Q_R and Q_P in the reference case. The patterns of both Q_R and Q_P are characterized by a series of cyclical (oscillating) events. These are fewer and less pronounced than the ones in the case of the deeper, warmer system of the *Moridis and Reagan*[8] study (in which they continued until the exhaustion of the hydrate). The constant-*P* depressurization results in an initial "burst" of gas release as the hydrate in the immediate vicinity of the well dissociates very rapidly. After this initial (and very short) explosive release stage, Q_R begins to increase quickly as hydrate saturation near the wellbore decreases through hydrate dissociation, increasing k_{eff}. The initial increasing trend is followed by a sharp decline in Q_R. As time progresses, each production cycle consists of a long stage of increasing Q_R, followed by a short stage of sharp decline. Q_P exhibits the same pattern. Additionally, the temporally local maxima and minima of Q_R and Q_P occur at the same times. The pattern is repeated until about t = 4,350 days, after which time (a) a very gradual decline in both Q_P and Q_R is observed, (b) the two follow very closely each other, with Q_R very slightly exceeding Q_P (indicating a virtual balance between production and release from dissociation). This is a direct consequence of the constant-*P* production regime, which constantly adjusts the production rates to reflect the different k_{eff} and pressure differential between the well and the HBL. At the end of the 30-year production period, over 60% of the hydrate remains in place, and Q_P = 0.68 ST m^3/s of CH_4 (2.08 MMSCFD).

Q_P in constant-*P* production begins in earnest from the moment depressurization is applied, and reaches high levels, with cycle maxima that reach 1.54 ST m^3/s of CH_4 (4.70 MMSCFD). Unlike the warmer deposits in the *Moridis and Reagan*[8] study (in which Class 3 hydrate deposits appeared to have a gas production potential that compares favorably with that of Class 2 accumulations), production is much lower under the shallower and colder conditions of the Ulleung Basin despite a thicker HBL. Although the Class 3 deposit produces at a significantly lower Q_P level than the equivalent Class 2 deposit we studied earlier in this paper, it can be more desirable at the early stages of production because of a high Q_P, and is not hampered by the cessation of production brought about by significant cooling. Figure 17 also shows the average gas production Q_{avg}, which reaches a maximum of 0.92 ST m^3/s (= 2.80 MMSCFD) during the 10,800-day production period. The wide oscillations at about *t* = 3,000 days and *t* = 3,500 days correspond to attempts to destroy secondary hydrate barriers[8].

Q_P never exceeds Q_R, indicating that gas production is not supported by the gas stored in the reservoir. This is evident in Figure 17, which shows V_R consistently exceeding V_P, indicating continuous storage of the extra released gas. As Figure 18 shows, at the end of the 10,800-day simulation period, a total of $V_P = 7.97\text{x}10^9$ ST m^3 ($2.81\text{x}10^{10}$ ST ft^3) have been produced, all of which originated from the hydrate. This is about half of what was produced from the much thinner (15m vs. 50m) but warmer formation of the *Moridis and Reagan*[8] study.

Figure 18 shows the water mass production rate Q_W at the well and the corresponding cumulative mass of produced water M_W. After the initial oscillations in each production cycle, the overall pattern shows an exponential decline of Q_W. At its peak immediately upon the initiation of production, Q_W = 10.4 kg/s (5,500 BPD), but it declines quickly. Even at its highest, Q_W is manageable, as is the cumulative mass of produced water M_W. Note that production from Class 3 hydrates by constant-*P* depressurization is at its most challenging upon initiation, and the picture continuously improves with time. This is the exact opposite of what happens in production from conventional gas reservoirs, and appears to be a significant advantage as it dictates planning for the worst-case scenario at the beginning rather toward the end of production.

Spatial distributions. Figures 19 and 20 show the evolution of the S_H and S_G spatial distributions over time in the very important zone (r < 50 m) around the wellbore[7,8]. These figures provide an explanation for the cyclical pattern of Q_R and Q_P observed in Figure 16. The precipitous drop in Q_R and Q_P is caused by the appearance of the *dual traveling barrier* that is formed from secondary hydrate around the well (Figure 19c). This feature is a typical response of the constant-P depressurization process[8], and is characterized by significant temperature drops within the inner "chamber" of the barrier (Figures 21e to 21f) where depressurization is at its most intense. Each of the precipitous Q_R and Q_P drops in Figure 16 occurs when the inner secondary hydrate barrier is formed and the traveling outer barrier is in place[8].

We attempted to destroy the dual traveling barrier by injecting warm water. Despite long injection times, it was not possible to fully destroy the barrier because of the adverse P regime in Class 3 deposits, which leads to flow stagnation of the injected fluid as it collides with the reservoir fluids moving in the opposite direction. Drainage and flow short-circuiting are quite common under these circumstances, and this what happened here. The small hydrate occurrences to the right of the clearly defined barriers in Figures 19d and 19e are the remnants of the unsuccessful attempts to destroy the barriers by water injection. The clearly defined vertical barriers in the same figures are newly formed structures that were created a few days after the end of the warm water injection.

What is particularly interesting is what happens past t = 3600 days, when no further attempt is made to destroy the barriers. The advance of the outermost traveling barrier slows down, it collides with the next one approaching from the well (Figure 19f), and the process is repeated until several of these structures collide and begin to fuse (Figure 19g). The fused structure continues to move away from the well, and its lower parts begin to disintegrate (Figure 19h). During all this times, gas continues to accumulate at the top of the HBL because of buoyancy, while flowing over, through and below the barriers toward the well (Figures 20a to 20h). In Figures 19h and 20h, we observe the beginning of the formation of a bridge between the slowly moving fused structure and the main body of the remaining hydrate, with the gas flow showing signs of constriction (Figure 20h). As was discussed in the study of the Class 2 deposit, the implication of the gas accumulation pattern in Figure 20 is that the existence of a confining overburden is a necessity for gas production from marine Class 3 deposits to avoid gas losses that can undermine the feasibility of the venture.

Sensitivity Analysis of Production From Class 3 Deposits in the Ulleung Basin

We investigated the sensitivity of gas production from the colder Class 3 deposits covered in this study to the initial hydrate saturation S_{H0}. The results of these analyses are presented in Figures 23 through 25.

Sensitivity to S_{H0}. Figure 23a shows the dependence of Q_P on S_{H0}. Under the conditions of the Ulleung basin, the lowest S_{H0} = 0.30 leads initially to a highest Q_P because of a higher initial k_{eff} that results to higher initial dissociation. However, the pattern is reversed at a later time because, after the initial burst of gas release and production, this system is burdened with the combined adverse effects of (a) a larger native aqueous phase saturation, (b) difficulty in gas accumulation because of the higher k_{eff}, and (b) low gas releases that are limited by resource availability.

This behavior of potential Class 3 deposits is also illustrated by the evolution of the cumulative volume of produced gas V_P (Figure 24a) which, for S_{H0} = 0.30, clearly shows the reversal from highest at early times, to lowest at later times. The S_{H0} = 0.50 has the largest V_P because, although the corresponding Q_P lags behind that for S_{H0} = 0.65, the early releases appear to have created a large gas bank that can supply production. These results indicate that the relationship between Q_P and S_{H0} is not monotonic (exhibiting a Q_P maximum for an S_{H0} that falls between the extremes of its range), in addition to being a function of time. Therefore, meaningful comparisons require a time frame for proper evaluation. Regarding the evaluation of gas production from such deposits using the absolute criterion, the V_P estimates over the 30-year production period are not very different for S_{H0} = 0.50 and S_{H0} = 0.65 (V_P = 8.38x10^8 ST m^3 vs. 7.97x10^8 ST m^3, respectively), and is lower for S_{H0} = 0.30 (V_P = 6.56x10^8 ST m^3). This indicates that a rather weak (sublinear) relationship between Q_P and S_{H0} under the conditions of the Ulleung basin.

The cumulative mass of produced water M_W follows a far more predictable pattern (Figure 24b), increasing monotonically with a decreasing S_{H0}. This leads to the water-to-gas ratio R_{WGC} of Figure 25a, which indicate that despite the apparent superiority of the S_{H0} = 0.50 system (as evaluated using the absolute criterion), the S_{H0} = 0.50 system has a slight edge when using the relative criterion because its lower overall gas production is balanced by a lower production of unwanted water. Obviously, the relative weight of the absolute and the relative criteria as evaluation tools for the assessment of the potential of Class 3 deposits is not established yet, and will be determined by the needs and priorities (economic, technical and regulatory) of producing organizations.

The effect of S_{H0} on the salinity in the produced water X_S is rather straightforward (Figure 15b). Generally speaking, unlike the milder salinity changes in the produced water of Class 2 deposits, the attributes of Class 3 deposits result is much stronger X_S changes because the amount of originally free native water is lower, while a larger portion of the total water inventory is associated with the hydrate (with no access to a saline water aquifer, as is the case in Class 2 deposits[7]). Because it is unlikely that biota will be able to tolerate the salinity changes indicated in Figure 25b, mixing at appropriate rates with ocean water may be necessary in order to meet regulatory standards of release near the ocean floor.

Sensitivity to k. When k is reduced to 2.5x10^{-13} m^2 (= 250 mD, 50% of its reference value), the production performance deteriorates, as evaluated using the absolute criterion and the results in Figures 23a and 24a. V_P is consistently and substantially lower than that for the reference case during the entire 30-year production period (albeit at a level higher than that indicated by the k reduction), and Q_P is lower for a very long time (t < 7,900 days). While the H_2O production is also reduced (see M_W in Figure 24b), the positive consequences of this reduction are outweighed by the decline in gas production.

This is reflected by the relative criterion of R_{WGC} (Figure 25a), which indicates measurably worse performance (compared to that of the reference case) during the entire production period. As expected, the slower dissociation (Figure 23a) and the lower water production (Figure 24b) lead to the milder decline in the X_S in Figure 25b.

Sensitivity to *T*. Figure 23b shows the dependence of Q_P on the hydrate stability, as quantified by the system temperature T (reduced by about 2.5 ^oC, as in the case of the Class 2 sensitivity analysis), while keeping P equal to the reference case. The colder and more stable system results in markedly (and consistently) lower Q_P and V_P than that in the reference case, while M_W in Figure 24b is also lower because of a lower k_{eff} in the presence of a hydrate that resists dissociation. The resulting R_{WGC} in Figure 25a shows a very strong early dependence on T (the highest among the perturbed parameters), indicating larger water production in more stable systems (as expected), and demonstrates the desirability of deposits near the equilibrium temperature as production targets. The effect of T on X_S (Figure 25b) is described by a milder decline than the reference case because of the slower dissociation and the reduced water production.

Sensitivity to L_W. Production performance was adversely affected when the well spacing increased from L_W = 100 ha (=250 acres) to L_W = 380 ha (=960 acres), as evaluated using the absolute criterion and the results in Figures 23b and 24. Q_P was initially lower than that in the reference case, but exceeded it after t = 6,600 days. Note that Q_P continued increasing even at the end of the production period because of a continuously increasing k_{eff}, while the larger size of the production area maintained the pressure differential between the well and the dissociation front at high levels. While V_P exceeded that of the reference case at the end of the production period (Figure 24a) and was the highest among the perturbed cases, this performance was marred by the largest M_W recorded in the Class 3 study (Figure 24b). The corresponding R_{WGC} (Figure 25a) is substantially higher than in the reference case, and has the highest long-term value (and consequently, the worst relative performance) of all other perturbation parameters for t > 3,200 days. Thus, as in production from Class 2 deposits, the smallest possible L_W should be used for optimal production from Class 3 deposits in the Ulleung Basin. As expected, because of the much larger M_w and the lower V_P, the reduction in X_S in Figure 25b is less pronounced than in the reference case.

Sensitivity to *n*. The effect of the exponent n of the relative permeability function (see Table 1) on the system performance was very pronounced. When n was increased from 3.57 to 4.50 (indicating a stronger relationship between saturation and relative permeability, and a lower k_{eff}), the gas production was the worst in the entire sensitivity analysis, as indicated by the lowest Q_P and V_P in Figures 23b and 24a, respectively. While water production (see M_w in Figure 24b) was also reduced, the reduction was insufficient to improve the performance of R_{WGC}, which was among the worst (especially in the long term) in the sensitivity analysis. An additional negative effect of the steeper relative permeability curve (i.e., the larger n) is the stronger decline in X_S, which has the second worst performance (Figure 25b). This is caused by the low k_{eff}, which inhibits the flow of the native saline water and its mixing with the fresh water released from dissociation.

Additional Important Issues

Implications of the evolution pattern of R_{WGC} over time. Review of the evolution of the R_{WGC} pattern over time in Figures 15a and 25a confirms an earlier observation[7,8] that a universal feature of the depressurization-based production from both Class 2 and Class 3 deposits is the continuously declining water production in proportion to the gas production. Under any of the conditions and production methods investigated in this study R_{WGC} is shown to decrease continuously and monotonically over time until the system is exhausted. This is in stark contrast to the reality in conventional gas reservoirs, in which R_{WGC} invariably increases over time. The obvious conclusion is that hydrate deposits reserve their worst performance for the initial stages of production, but then they rapidly and continuously improve over time.

Uniformity of system response away from the well. The simulation of production from hydrates is controlled by processes and phenomena that occur within a critical radius around the well (i.e., r_c < 15-20 m) and require fine discretization to accurately capture and describe them. Dissociation and flow patterns are uniform and smooth for $r > r_c$. The reasons for this uniformity have been previously discussed by *Moridis and Reagan*[7,8]. Figures 26 and 27 confirm this uniformity in the reservoir-scale distributions of S_H and T during production from the reference cases of the Class 2 and Class 3 accumulations in the Ulleung Basin. Both figures show uniform dissociation patterns and smooth gradients along the entire reservoir radius r_{max}.

Summary and Conclusions

(1) We investigated gas production from potential hydrate deposits in the Ulleung basin of the Korean East Sea. We focused on the most likely types of hydrate deposits, and investigated the various factors and issues that may affect production from them. To evaluate the production potential we used an absolute criterion (based on the magnitude of the water and gas production), and a relative criterion that was based on the water-to-gas ratio. Additionally, we monitored the salinity of the produced water because of its cost, energy demand, and environmental implications.

(2) We focused on the hydrate deposit classes that are most likely to occur at the site and have the potential of becoming production targets, i.e., Classes 2 and 3. These are two most common classes of hydrate deposits in both the permafrost and in the oceans. Depressurization was selected as the main dissociation method because of its simplicity and effectiveness.

(3) The well design used for the constant-Q_M production from the Class 2 deposit at the Ulleung Basin involved different configurations of perforated intervals and warm water injection at different phases of the production

process. This well design prevented the formation of secondary hydrate and/or ice, and ensured continuous access of the gas evolving from dissociation to the well (induced by constant-Q_M and constant-P production from

(4) In the absence of any field measurements, we used simple principles of hydrate science and thermodynamics to develop fairly good estimates of the initial conditions in the Class 2 system under study. These estimates were based on the system geometry, the elevation at the base of the hydrate layer, the equilibrium temperature at that point, the general tendency of hydrate deposits to follow the hydrostatic gradient, and estimates of the geothermal gradient and/or of the temperature at the sea floor.

(5) The initial mass withdrawal rate Q_{M0} (= 36.8 kg/s = 20,000 BPD) was set high for optimal production performance. Q_M was continuously adjusted to prevent cavitation. Unlike the case of deeper, warmer systems, production could not be maintained until the exhaustion of the hydrate because very low temperatures in the HBL forced the cessation of production after about 10 years o production. Because a large fraction of the original hydrate (about 50%) remains in the reservoir, a potential production option involves the interruption of production for sufficiently long periods (1 year or more) to allow the thermal recovery of the hydrate (with the geothermal gradient replenishing the depleted heat reservoir in the HBL) before resuming production. However, no definitive conclusions can be reached because the subject has by no means been thoroughly researched.

(6) During the 10 years of continuous production prior to cessation, Q_P from a single vertical well in the reference case of the Class 2 Ulleung deposit reached a maximum of 3.07 ST m^3/s (= 9.37 MMSCFD), and production average Q_{avg} =2.00 ST m^3/s = 6 MMSCFD. During this period, a total of V_P = 6.67x10^8 ST m^3 (= 2.35x10^{10} ST ft^3) of CH_4 were produced.

(7) Sensitivity analysis indicated that gas production from such a system increased with (i) a decreasing S_{H0}, (ii) an increasing k, (iii) increasing T, (iv) an increasing Q_M, and (v) a decreasing well spacing L_W. Accounting for the concurrent water production, the most desirable production targets involve Class 2 deposits with low S_{H0}, which appear to yield in the most promising long-term water-to-gas ratio R_{WGC}. The effect of various parameters and conditions on the salinity of the released water is mild, and may allow water releases near the ocean floor without the risk of adversely affecting chemosynthetic communities and other biota.

(8) Production from Class 3 deposits in the Ulleung basin involved a simple well design and a constant-P regime at the well. The bottomhole constant pressure P_w = 2.8 MPa > P_Q, thus eliminating the possibility of ice formation and the corresponding potentially adverse effect on k_{eff}.

(9) In Class 3 deposits, production continued uninterrupted for 30 years, and was characterized by a series of initial oscillations, followed by a long period of mild decline in Q_P. These early oscillations corresponded to formation and destruction of secondary hydrate barriers. The maximum Q_P = 1.54 ST m^3/s (4.70 MMSCFD), and the average production rate from a single vertical well in over the 10,800-day period was Q_{avg} = 0.92 ST m^3/s (2.80 MMSCFD). A total of V_P = 7.97x10^9 ST m^3 (2.81x10^{10} ST ft^3) were produced, all of which originated from the hydrate. This is about half of what was produced from the much thinner (15m vs. 50m) but warmer formation of the *Moridis and Reagan*[8] study.

(10) Sensitivity analysis indicated that gas production from such a Class 3 system increased with (i) an increasing k, (ii) an increasing T, (iii) a decreasing well spacing L_W, and (iv) a decreasing n. Gas production from such a system is a complex function of S_{H0} and of the time frame of production. Generally, Q_P increased with a decreasing S_{H0} at early times, but the trend was reversed later. The situation becomes even more complicated when water production is considered. Consequently, the evaluation of the desirability of such deposits as production targets is not a straightforward proposition, but will need to involve consideration of the expected time frame of operation and of various production performance criteria. The reduction in the salinity of the released water is considerably larger than in the case of Class 2 deposits, indicating the need to consider the environmental implications of water releases.

(11) In both classes, dissociation is characterized by features that are common to all deposits: (a) the evolution of an upper dissociation interface at the top of the hydrate layer (caused by heat flows from the upper boundary) in addition to the lower dissociation interface at the bottom of the HBL, and (b) gas accumulation below the base of the overburden because of continuing dissociation and buoyancy-driven gas rise to the top of the formation. This gas accumulation pattern underlines the importance of a confining overburden as a critical component for the technical viability of a gas production scheme from hydrate deposits.

(12) Under the conditions of the Ulleung basin, and for the well configurations employed for production, practically no secondary hydrate was observed during production from Class 2 deposits. Traveling barriers that fused over time emerged during production from Class 3 deposits, but these did not halt production.

(13) This study confirms earlier observations that dissociation and flow patterns are uniform and smooth along the entire area of the horizontal interfaces away from a narrow zone around the well. This critical zone has a radius r_c < 15-20 m, and fine discretization must be used in its simulations if these near-well phenomena are to be captured and accurately described.

(14) This study also confirmed another earlier observation, namely that gas production from hydrates under any of the conditions and production methods is characterized by a continuous and monotonic decline of the water-to-gas ratio. This is in stark contrast to the performance of conventional gas reservoirs. The obvious conclusion is that hydrate deposits reserve their worst performance for the initial stages of production, but then they rapidly and continuously improve over time.

Nomenclature

Δr = Radial increment (m)
Δt = Timestep size (s)
Δz = Vertical discretization, i.e., in the *z*-direction (m)
C = specific heat (J/kg/K)
k = intrinsic permeability (m^2)
k_Θ = thermal conductivity (W/m/K)
$k_{\Theta RD}$ = thermal conductivity of dry porous medium (W/m/K)
$k_{\Theta RW}$ = thermal conductivity of fully saturated porous medium (W/m/K)
M_W = cumulative mass of water released into the ocean through the annular gravel pack (kg)
N_H = hydration number
P = pressure (Pa)
P_0 = initial pressure in hydrate-bearing sediments (Pa)
Q_Θ = rate of heat injection into the formation next to the well (W/m of wellbore)
Q_I = mass rate of injected warm water at the well (kg/s)
Q_M = mass rate of fluid withdrawal at the well (kg/s)
Q_P = volumetric rate of CH_4 production at the well (ST m^3/s)
Q_R = volumetric rate of CH_4 release from hydrate dissociation into the reservoir (ST m^3/s)
Q_W = mass rate of water release into the ocean through the annular gravel pack (kg/s)
Q_V = rate of CH_4 release from hydrate dissociation (ST m^3/s)
r,z = coordinates (m)
r_c = critical radius of maximum activity around the wellbore (m)
r_w = radius of the well assembly (m)
r_{max} = maximum radius of the simulation domain (m)
R_{WGC} = cumulative water-to-gas ratio (kg/ST m^3)
S = phase saturation
t = time (days)
T = temperature (K or ^oC)
V_R = cumulative volume of CH_4 released from hydrate dissociation (ST m^3)
V_P = cumulative volume of CH_4 released into the ocean through the annular gravel pack (ST m^3)
X = mass fraction (kg/kg)

Greek Symbols

λ = van Genuchten exponent – Table 1
ϕ = porosity

Subscripts and Superscripts

0 = denotes initial state
A = aqueous phase
e = equilibrium conditions
cap = capillary
G = gas phase
G0 = initial gas phase
H = solid hydrate phase
H0 = initial solid hydrate phase
irG = irreducible gas
irA = irreducible aqueous phase
n = permeability reduction exponent – Table 1
P = production stream
S = salinity
ref = reference Case C
R = rock

Acknowledgment

This work was supported by the Korea Institute of Geoscience and Mineral Resources, and by the Assistant Secretary for Fossil Energy, Office of Natural Gas and Petroleum Technology, through the National Energy Technology Laboratory, under the U.S. Department of Energy, Contract No. DE-AC02-05CH11231. The authors are indebted to Stefan Finsterle, John Apps and Dan Hawkes for their thorough review and their insightful comments.

References

1. Sloan, E.D., *Clathrate Hydrates of Nautral Gases.* Marcel Decker, Inc., New York, NY (1998).
2. Milkov, A. V., “Global estimates of hydrate-bound gas in marine sediments: How much is really out there,” *Earth Science Reviews* **66**(3), 183 (2004).
3. Klauda, J.B., Sandler, S.I., “Global distribution of methane hydrate in ocean sediment,” *Energy & Fuels* **19**, 469 (2005).
4. Makogon, Y.F., “Gas hydrates: frozen energy,” *Recherche* **18**(192), 1192 (1987).
5. Dallimore, S.R., Collett, T.S., Eds., “Scientific Results from the Mallik 2002 Gas Hydrate Production Research Well Program, Mackenzie Delta, Northwest Territories, Canada,” *Geological Survey of Canada Bulletin* **585** (2005).
6. Moridis, G.J., Kowalsky, M.B., Pruess, K., “Depressurization-Induced Gas Pproduction From Class 1 Hydrate Deposits,” (LBNL-59780) SPE 97266, 2005 SPE Annual Technical Conference and Exhibition, Dallas, Texas, U.S.A., October 9-12, 2005.
7. Moridis, G.J., Reagan, M.T., “Gas Production From Oceanic Class 2 Hydrate Accumulations,” OTC 18866, 2007 Offshore Technology Conference, Houston, Texas, U.S.A., 30 April–3 May 2007.
8. Moridis, G.J., Reagan, M.T., “Strategies for Gas Production From Oceanic Class 3 Hydrate Accumulations,” OTC 18865, 2007 Offshore Technology Conference, Houston, Texas, U.S.A., 30 April–3 May 2007.
9. Moridis, G.J., Sloan, E.D., “Gas Production Potential of Disperse Low-Saturation Hydrate Accumulations in Oceanic Sediments,” (LBNL-52568) *J. Energy Conversion & Management*, **48**(6), 1834-1849, doi: 10.1016/j.enconman.2007. 01.023 (2007).
10. Kurihara, M., Funatsu, K., Ouchi, H., Masuda, Y., Narita, H.: “Investigation of Applicability of Methane Hydrate Produ-ction Methods to Reservoirs With Diverse Characteristics”, Paper 3003, in *Proceedings of the 5th International Conference on Gas Hydrates,* June 13–16, Trondheim, 714 (2005).
11. Hong, H., Pooladi-Darvish, M.: “Simulation of Depressurization for Gas Production from Gas Hydrate Reservoirs,” *J. Can. Pet. Tech.*, **44**(11), 39 (2005).
12. Chough, S.K., Lee, H.J., Yoon, S. H., *Marine Geology of Korean Seas* (Second Edition), Elsevier, Amsterdam (2000) 313.
13. Ryu, B.J., Lee, Y.J., Kim, J.H., Kim, I.S., Park, M.H., “Geological and geothermal indicators for natural gas hydrates in shallow sediments of the Western Ulleung Basin, East Sea”, *Proceedings of the International Symposium on Gas Hydrate Technology*, Seoul, Korea, Nov. 10-11 (2005) 38.
14. Ludwig, W.J., Murauchi, S., Houtz, R.E., “Sediments and Structures of the Japan Sea”, *Geol. Soc. Am. Bull*., (1975) 86, 651.

15. Park, K.S., “Geological Structure and Seismic Stratigraphy of the southern part of the Ulleung Basin”, in Chough, S.K. (Ed.), *Sedimentary Basins in the Korean Pennisula and Adjacent Seas*, Hanlimwon Publishers, Seoul (1992) 40.
16. Kwon, Y.K., Chough, S.K., “Seismic Stratigraphy of the Ulleung Basin, East Sea”, *Proceedings of the International Symposium on Gas Hydrate Technology*, Seoul, Korea, Nov. 10-11 (2005) 53.
17. Park, K.P., “Gas Hydrate Exploration in Korea”, *Proceedings of the 2nd International Symposium on Gas Hydrate Technology*, Daejeon, Korea, Nov. 1-2 (2006) 24.
18. Makogon, Y.F., *Hydrates of Hydrocarbons*. Penn Well Publishing Co. Tulsa, OK. (1997).
19. Moridis, G.J., Kowalsky, M.B., “Gas Production from Unconfined Class 2 Hydrate Accumulations in the Oceanic Subsurface,” (LBNL-57299) in *Economic Geology of Natural Gas Hydrates*, M. Max, A.H. Johnson, W.P. Dillon and T. Collett, Eds., Kluwer Academic/Plenum Publishers (2006).
20. Moridis, G.J., Kowalsky, M.B., Pruess, K., “TOUGH-Fx/HYDRATE v1.0 User’s Manual: A Code for the Simulation of System Behavior in Hydrate-Bearing Geologic Media,” Report LBNL-58950, Lawrence Berkeley National Laboratory, Berkeley, CA (2005).
21. Kim, H.C., Bishnoi, P.R., Heidemann, R.A., and Rizvi, S.S.H.: “Kinetics of Methane Hydrate Decomposition”, *Chem. Eng. Sci*., **42**(7), 1645 (1987).
22. Clarke, M.A., and Bishnoi, P.R.: “Determination of the Intrinsic Rate of Methane Gas Hydrate Decomposition”, *Chem. Eng. Sci.*, **55**, 4869 (2000).
23. Wright, J.F., Dallimore, S.R., and Nixon, F.M.: “Influences of Grain Size and Salinity on Pressure-Temperature Thresholds for Methane Hydrate Stability in JAPEX/JNOC/GSC Mallik 2L-38 Gas Hydrate Research-Well Sediments”, in Scientific Results from JAPEX/JNOC/GSC Mallik 2L-38 Gas Hydrate Research-Well, Mackenzie Delta, Northwest Territories, Canada. Dallimore, S.R., Uchida, T., and Collett, T.S., Eds., *Geological Survey of Canada Bulletin* **544**, 229 (1999).
24. Moridis, G.J., Seol, Y., Kneafsey, T., “Studies of Reaction Kinetics of Methane Hydrate Dissociation in Porous Media”, (LBNL-57298) Proc. 5th International Conference on Gas Hydrates, Trondheim, Norway, June 13-16, 2005, Paper 1004, **1**, 21-30 (2005).
25. van Genuchten, M.Th.: “A Closed-Form Equation for Predicting the Hydraulic Conductivity of Unsaturated Soils”, *Soil Sci. Soc.*, **44**, 892 (1980).

Table 1 – Hydrate Deposit Properties

Parameter	Value
Water zone (WZ) thickness (Class 2)	15 m
Hydrate zone (HBL) thickness	50 m
Initial pressure P_B (at base of HBL)	2.045×10^7 Pa
Initial temperature T_B (at base of HBL)	286.4 K (13.24 ^{o}C)
Gas composition	100% CH_4
Initial saturations in the HBL	$S_H = 0.65$, $S_A = 0.35$
Water salinity (mass fraction)	0.035
Intrinsic permeability k_r=k_z (HBL and water zone)	5×10^{-13} m^2 (= 0.5 D)
Intrinsic permeability k_r=k_z (overburden & underburden)	0 m^2 (= 0 D)
Grain density ρ_R (HBL and WZ)	2750 kg/m^3
Porosity ϕ (HBL and WZ)	0.35
Initial mass production rate Q_{M0}	37.91 kg/s (= 20,000 BPD)
Dry thermal conductivity $k_{\Theta RD}$ (all formations)	1.0 W/m/K
Wet thermal conductivity $k_{\Theta RW}$ (all formations)	3.1 W/m/K
Composite thermal conductivity model[24]	$k_{\Theta C} = k_{\Theta RD} + (S_A^{1/2} + S_H^{1/2})\ (k_{\Theta RW} - k_{\Theta RD}) + \phi S_I k_{\Theta I}$
Capillary pressure model[25]	$P_{cap} = -P_0 \left[(S^*)^{-1/\lambda} - 1 \right]^{\lambda}$ $S^* = \frac{(S_A - S_{irA})}{(S_{mxA} - S_{irA})}$
S_{irA}	1
λ	0.45
P_0	10^5 Pa
Relative permeability Model	$k_{rA} = (S_A*)^n$ $k_{rG} = (S_G*)^n$ $S_A* = (S_A - S_{irA})/(1 - S_{irA})$ $S_G* = (S_G - S_{irG})/(1 - S_{irA})$ OPM model
n (from Moridis et al.[20])	3.572
S_{irG}	0.02
S_{irA}	0.25

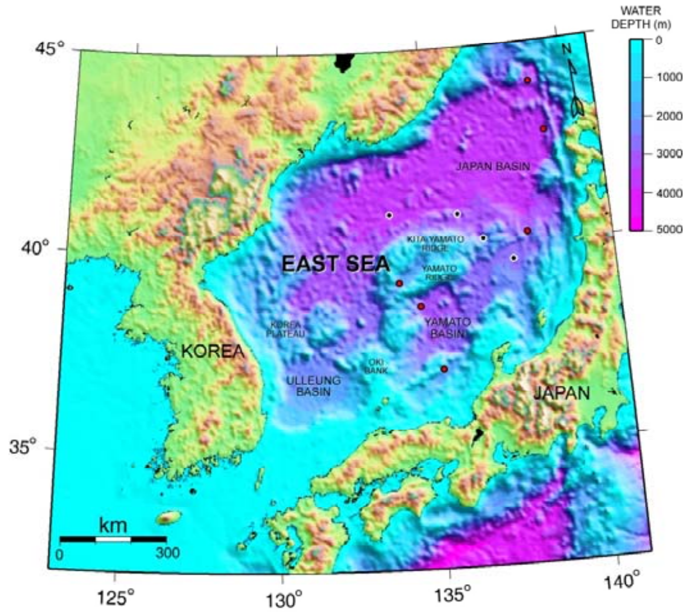

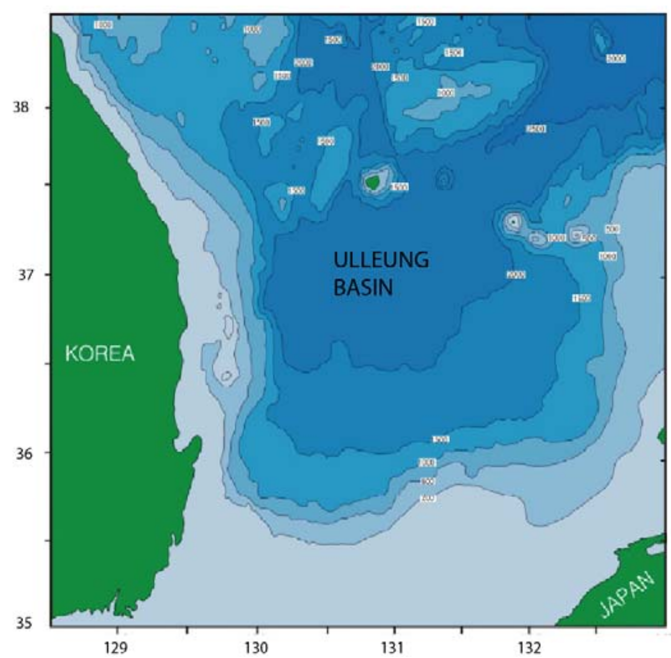

Figure 1 – Physiographic map of the Ulleung Basin[13].

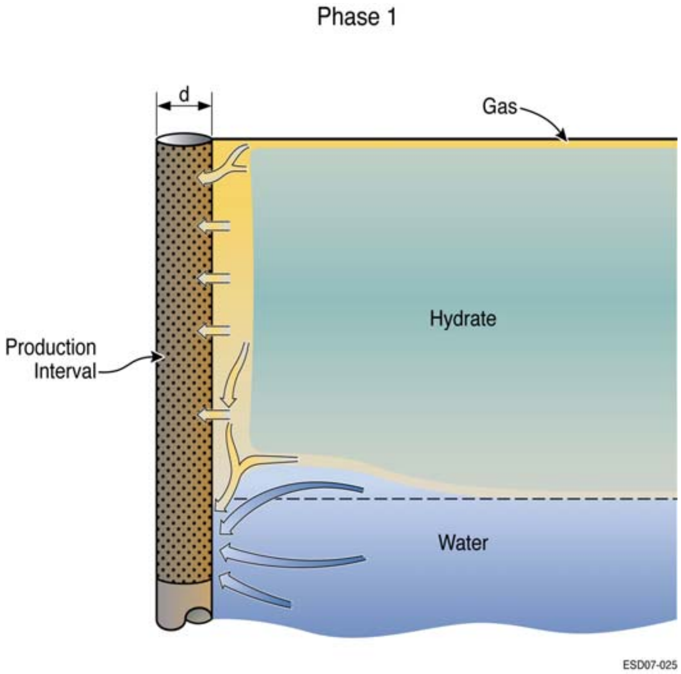

Figure 2 – Well design used in the initial phase of gas production from a Class 2 deposit in the Ulleung Basin. The production interval covers the entire HBL and extends into the WZ.

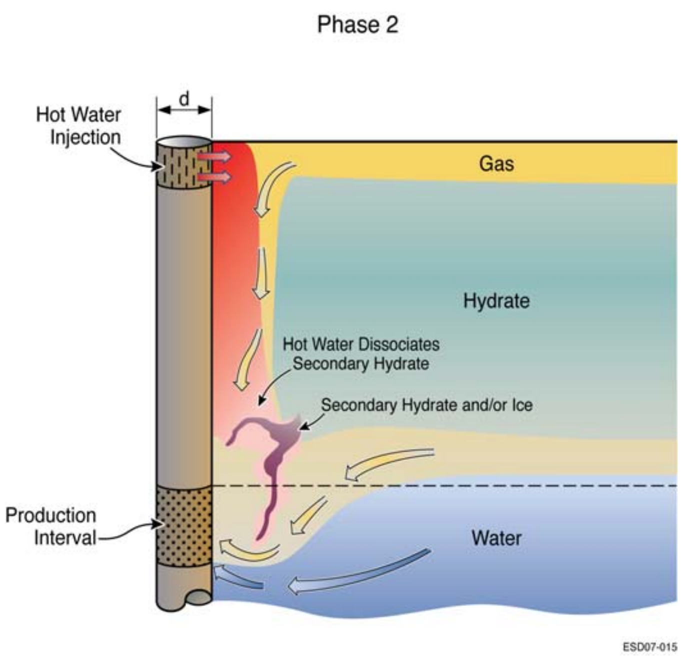

Figure 3 – Well design variant used in the early and intermediate production stages of Case C in this study. Warm water is injected into the formation near the top of the perforated interval.

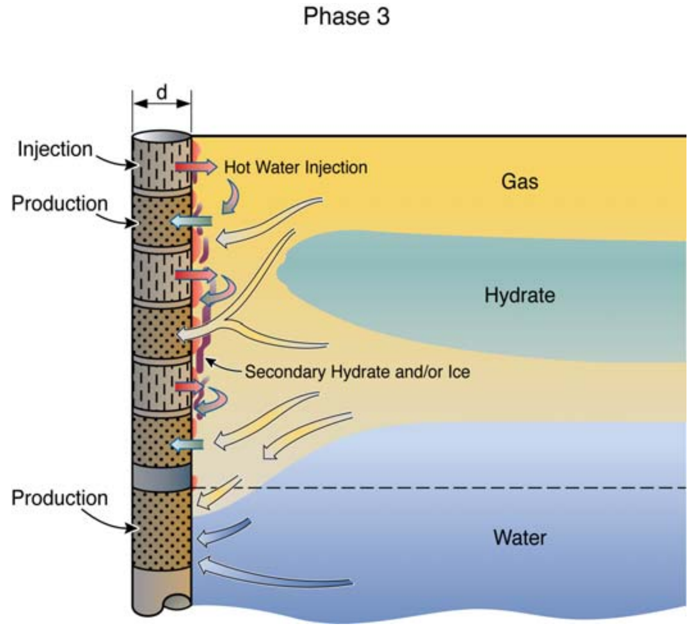

Figure 4 – Well design used in the late stages of production in Case C[7]. The system involves thin alternating zones of production and warm water injection.

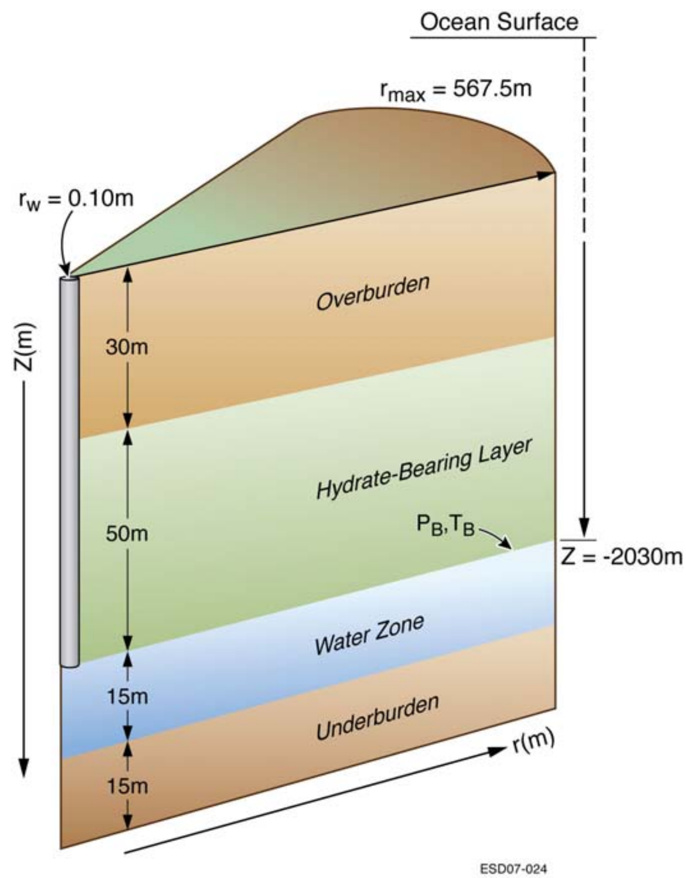

Figure 5 – A schematic of the marine Class 2 hydrate deposit simulated in this study.

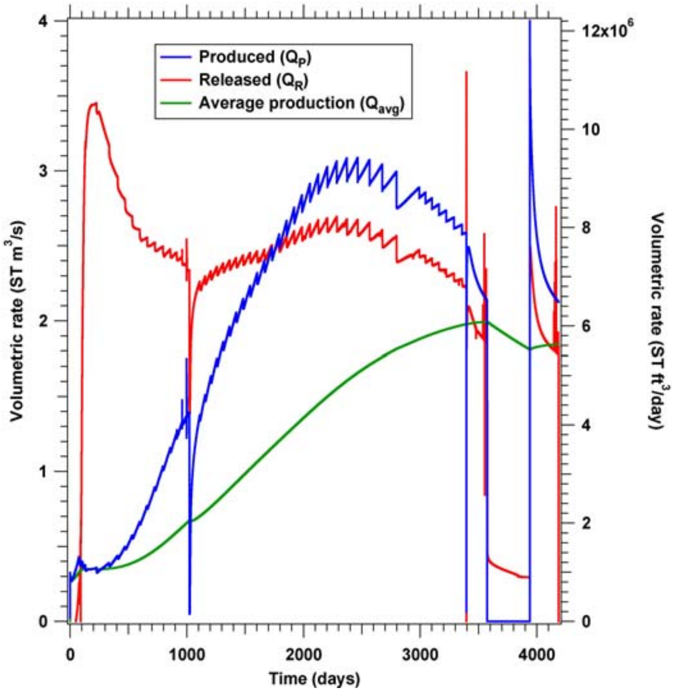

Figure 6 – Rates of (a) hydrate-originating CH_4 release in the reservoir (Q_R) and (b) CH_4 production at the well (Q_P) during production from a marine Class 2 hydrate deposit in the Ulleung Basin. The average production rate (Q_{avg}) over the simulation period is also shown.

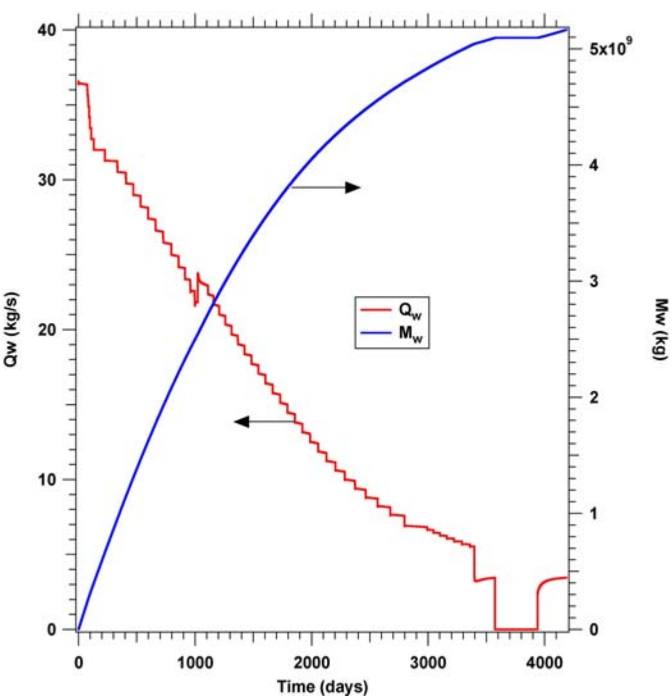

Figure 7 – (a) Rate of H_2O production (Q_W) and (b) cumulative mass of produced H_2O (M_W) during production from the marine Class 2 hydrate deposit in this study.

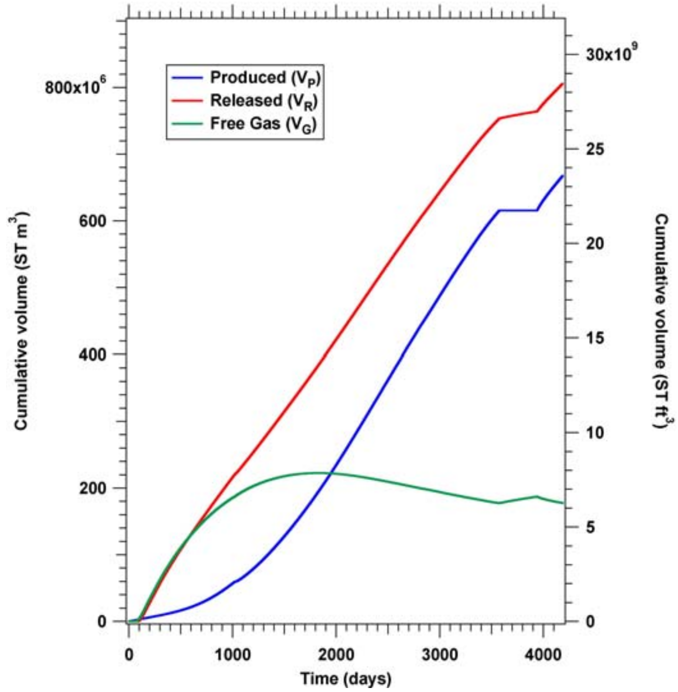

Figure 8 – Cumulative volumes of (a) hydrate-originating CH_4 released in the reservoir (V_R) and (b) produced CH_4 at the well (V_P) during production from the marine Class 2 hydrate deposit in this study.

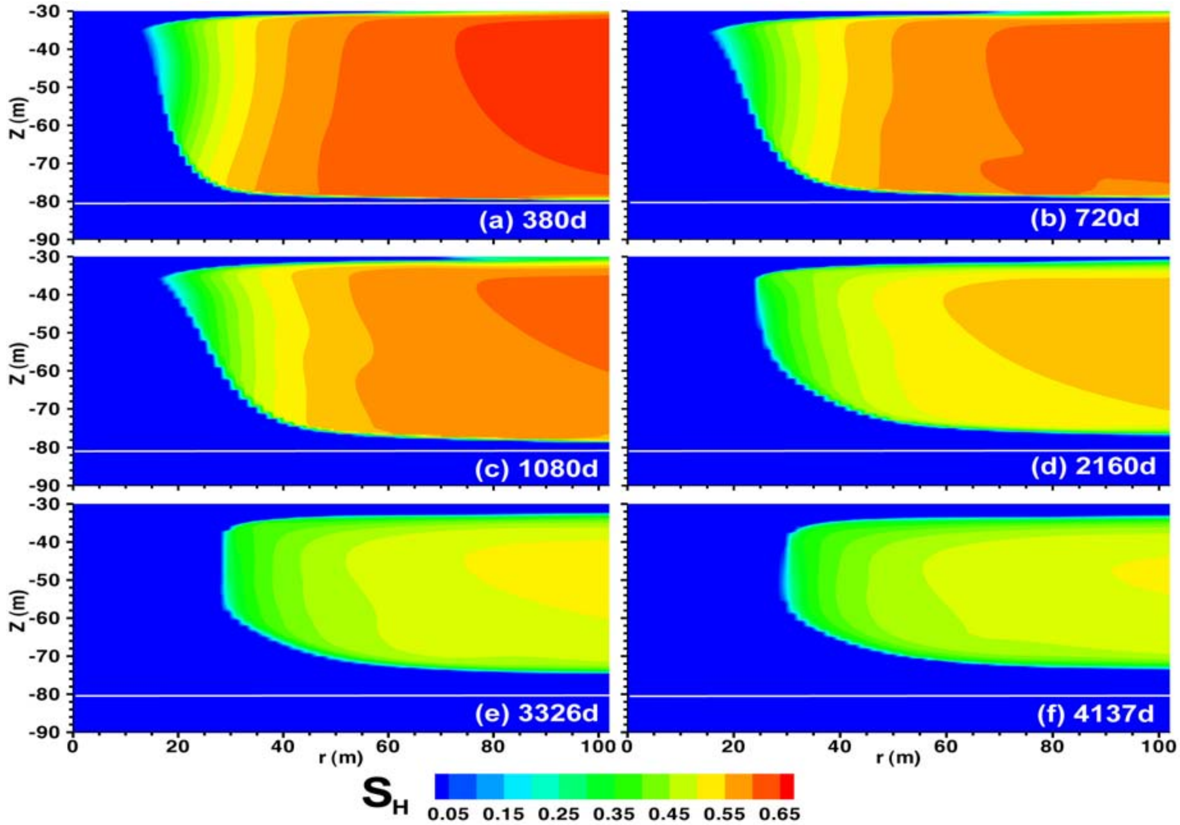

Figure 9 – Evolution of spatial distribution of S_H during gas production from the marine Class 2 hydrate deposit in this study.

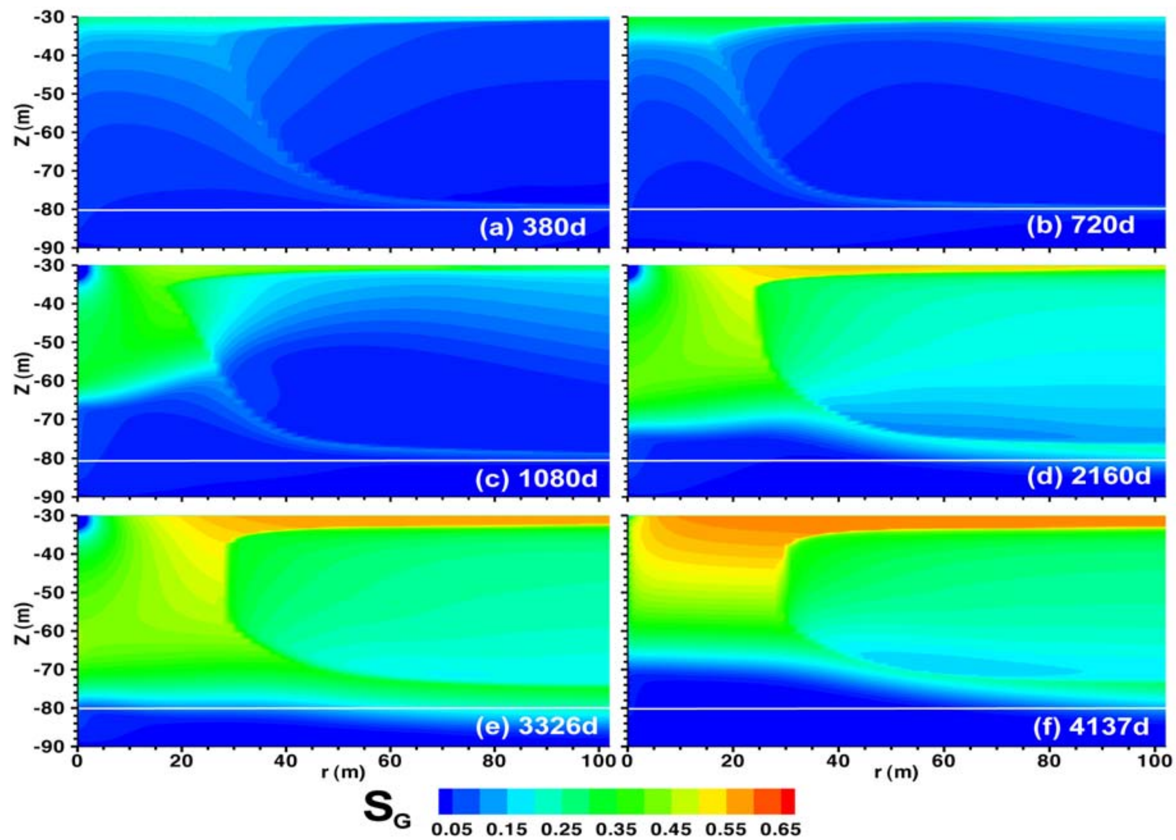

Figure 10 – Evolution of spatial distribution of S_G during gas production from the marine Class 2 hydrate deposit in this study.

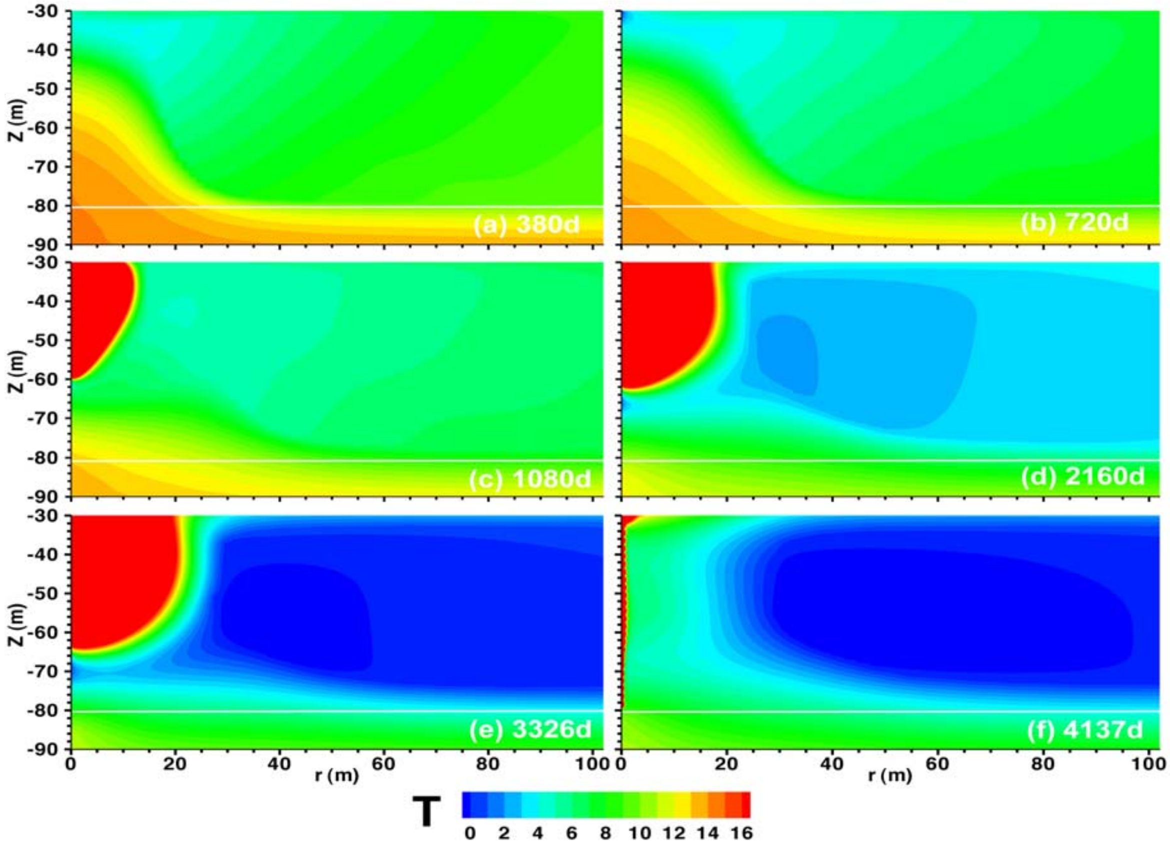

Figure 11 – Evolution of spatial distribution of T during gas production from the marine Class 2 hydrate deposit in this study.

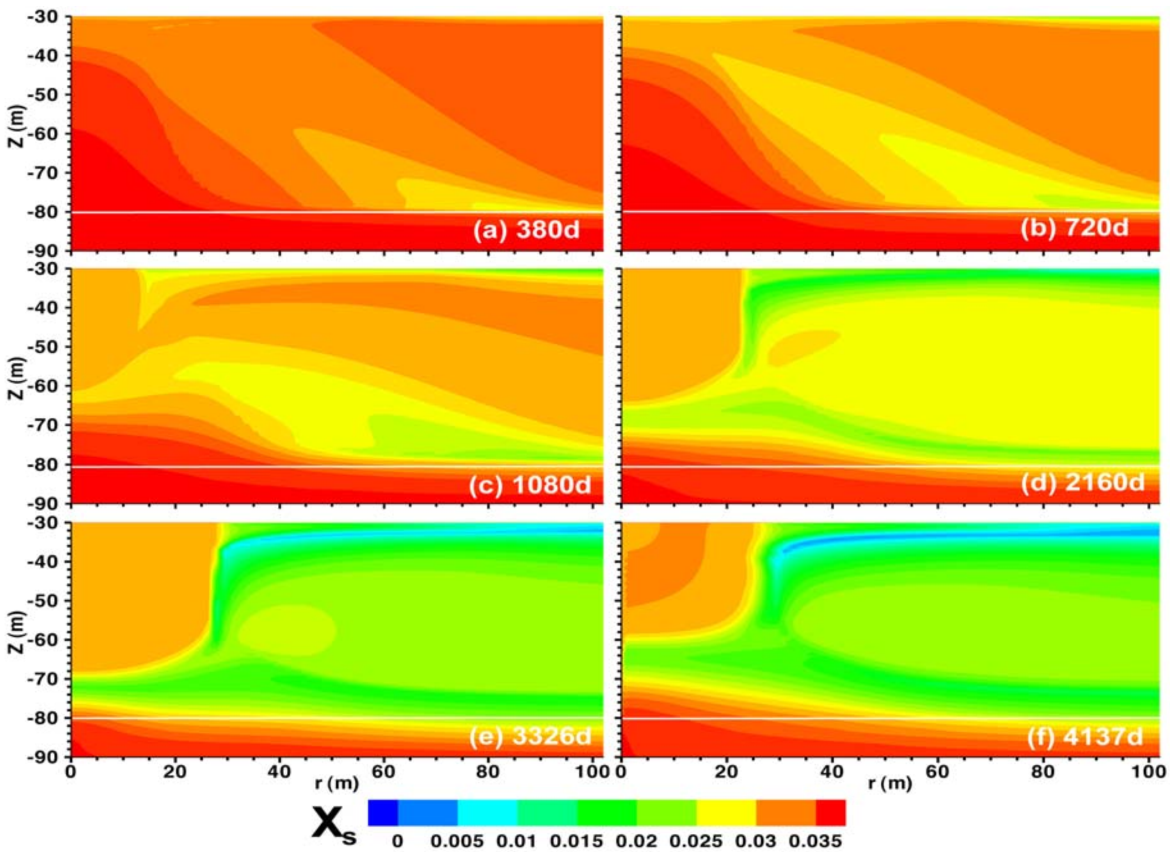

Figure 12 – Evolution of spatial distribution of X_S during gas production from the marine Class 2 hydrate deposit in this study.

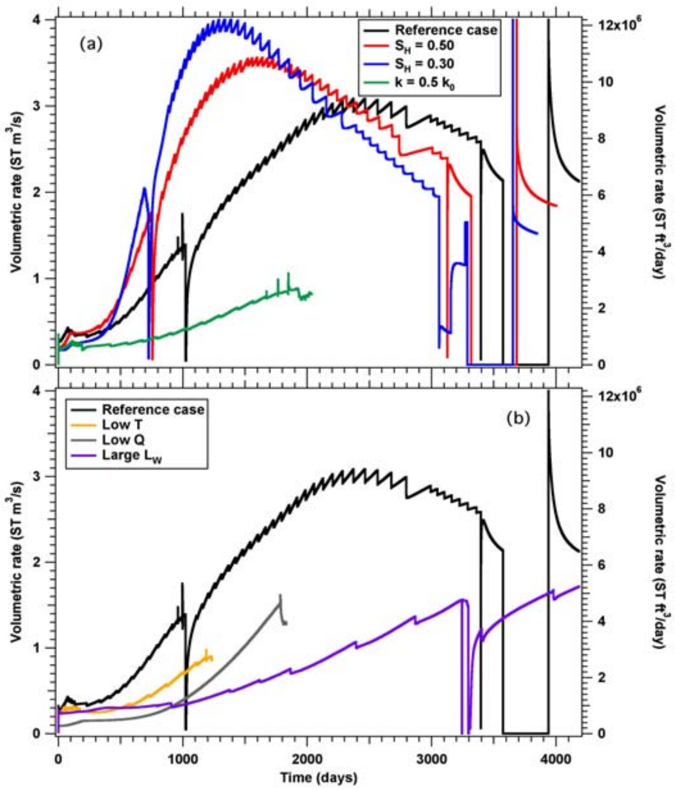

Figure 13 – Sensitivity analysis: effect of various perturbation parameters on the evolution of Q_P during production from the marine Class 2 hydrate deposit in this study.

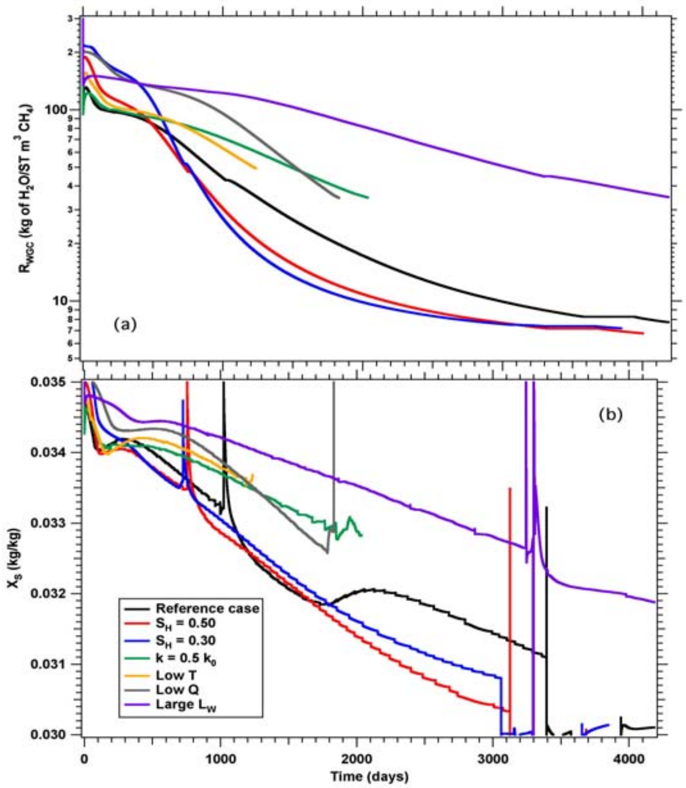

Figure 15 – Sensitivity analysis: effect of various perturbation parameters on the evolution of R_{WGC} and X_P during production from the marine Class 2 hydrate deposit in this study.

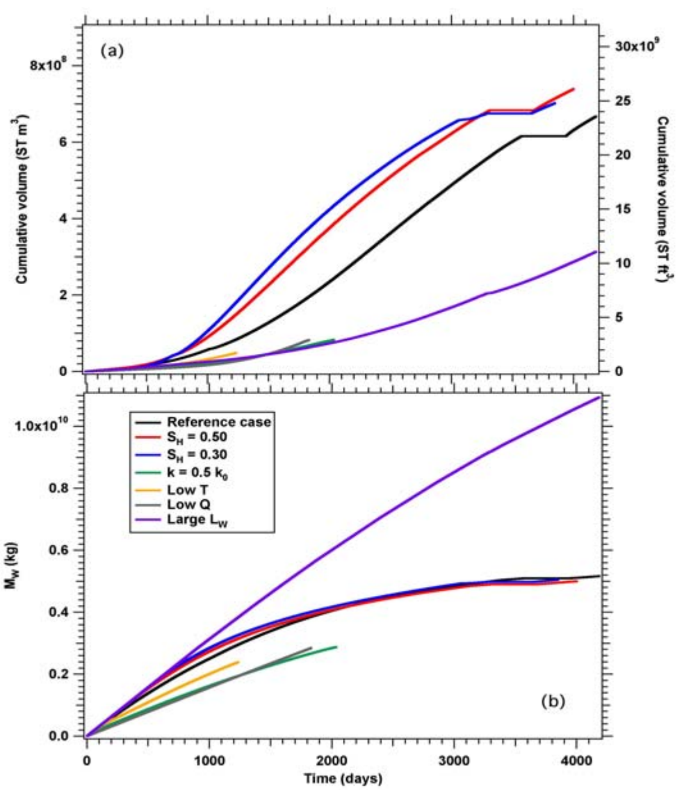

Figure 14 – Sensitivity analysis: effect of various perturbation parameters on the evolution of V_P and M_W during production from the marine Class 2 hydrate deposit in this study.

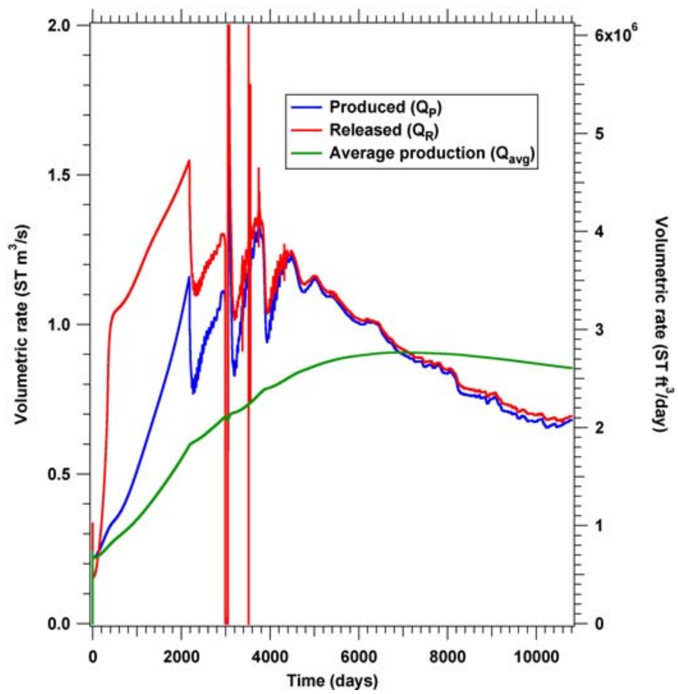

Figure 16 – Rates of (a) hydrate-originating CH_4 release in the reservoir (Q_R) and (b) CH_4 production at the well (Q_P) during production from marine Class 3 hydrate deposit in in the Ulleung Basin. The average production rate (Q_{avg}) over the simulation period is also shown.

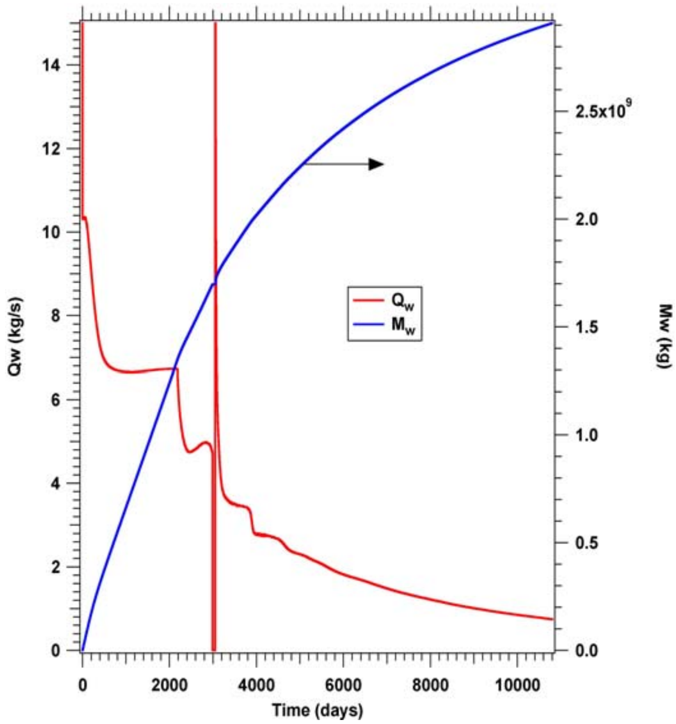

Figure 17 – (a) Rate of H_2O production (Q_W) and (b) cumulative mass of produced H_2O (M_W) during production from the marine Class 3 hydrate deposit in this study.

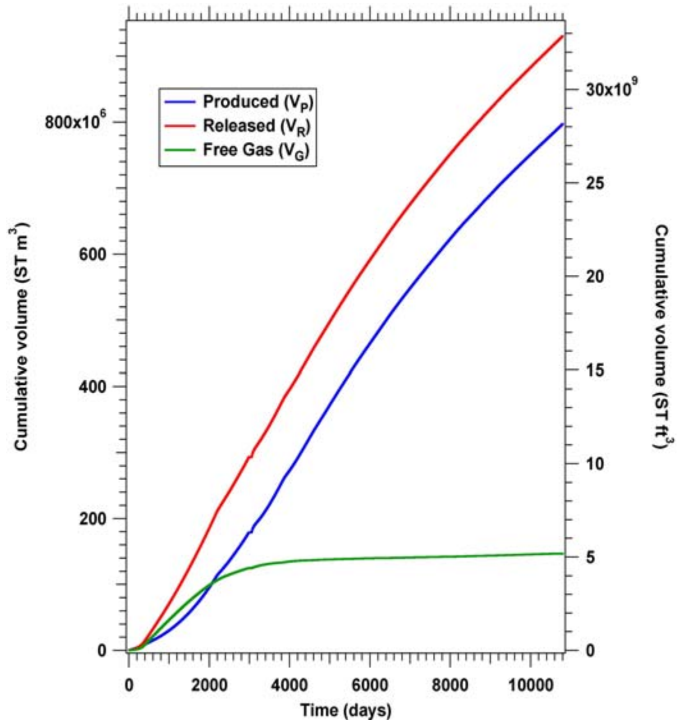

Figure 18 – Cumulative volumes of (a) hydrate-originating CH_4 released in the reservoir (V_R) and (b) produced CH_4 at the well (V_P) during production from the marine Class 3 hydrate deposit in this study

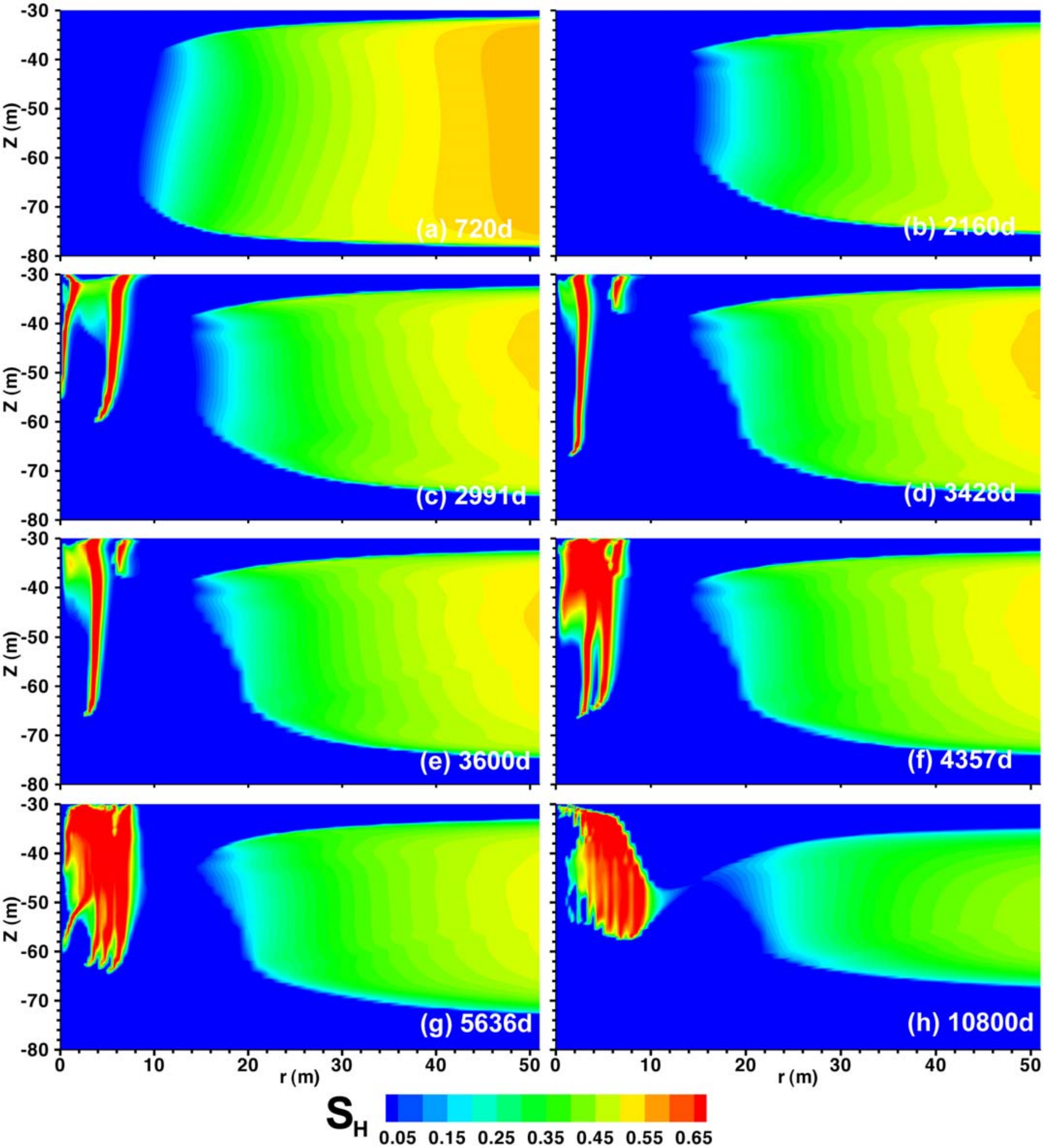

Figure 19 – Evolution of spatial distribution of S_H during gas production from the marine Class 3 hydrate deposit in this study.

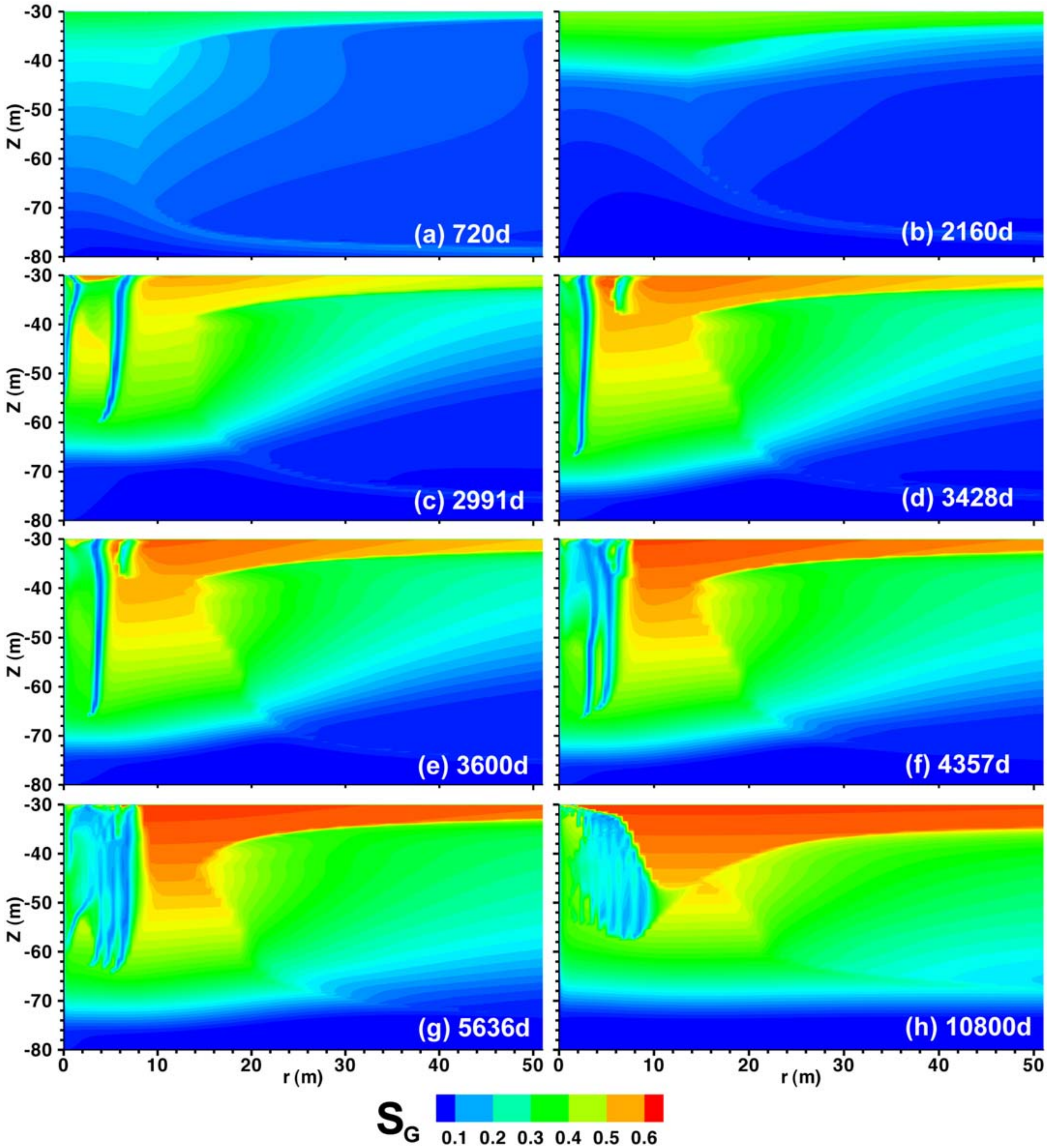

Figure 20 – Evolution of spatial distribution of S_G during gas production from the marine Class 3 hydrate deposit in this study.

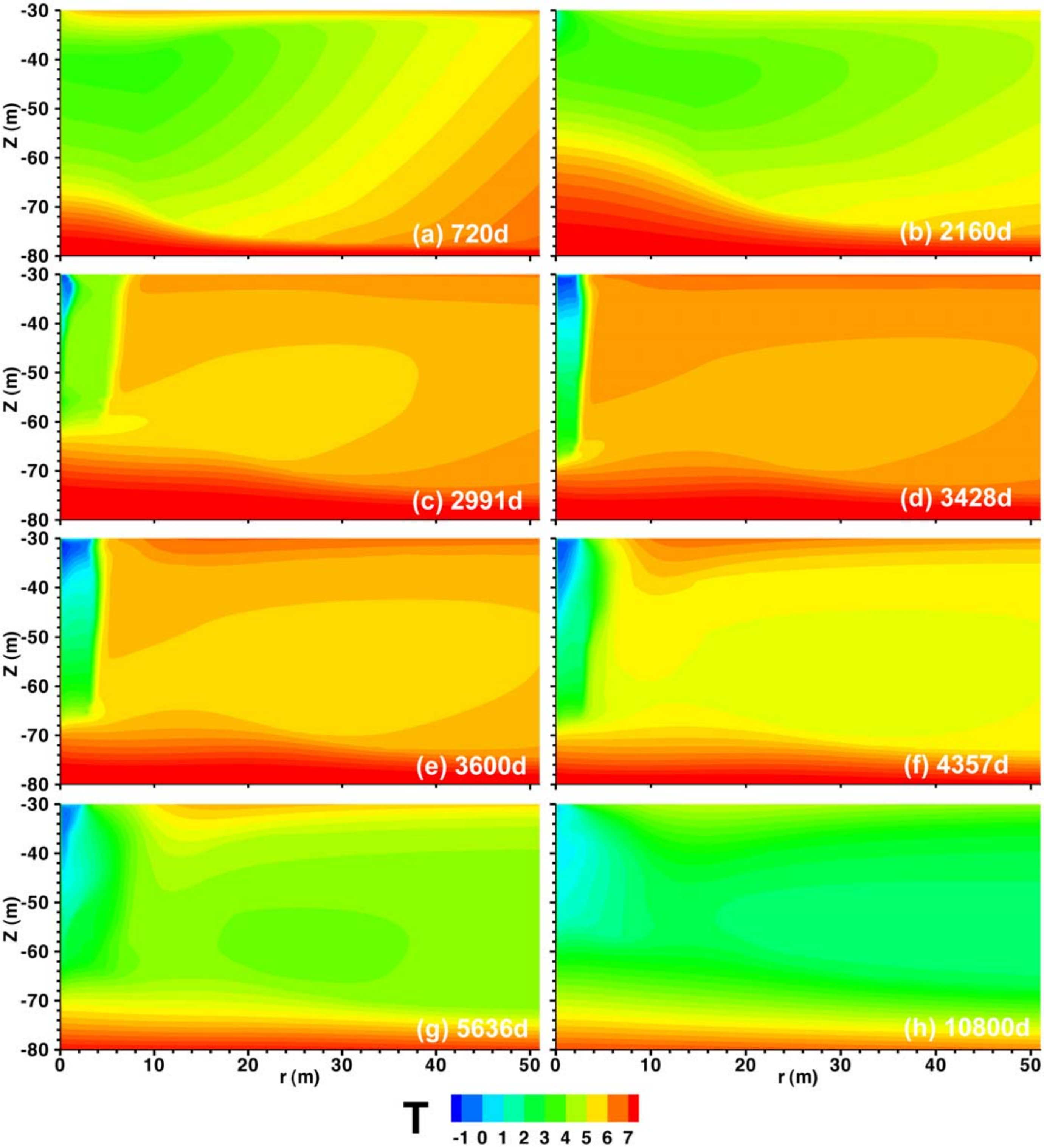

Figure 21 – Evolution of spatial distribution of T during gas production from the marine Class 3 hydrate deposit in this study.

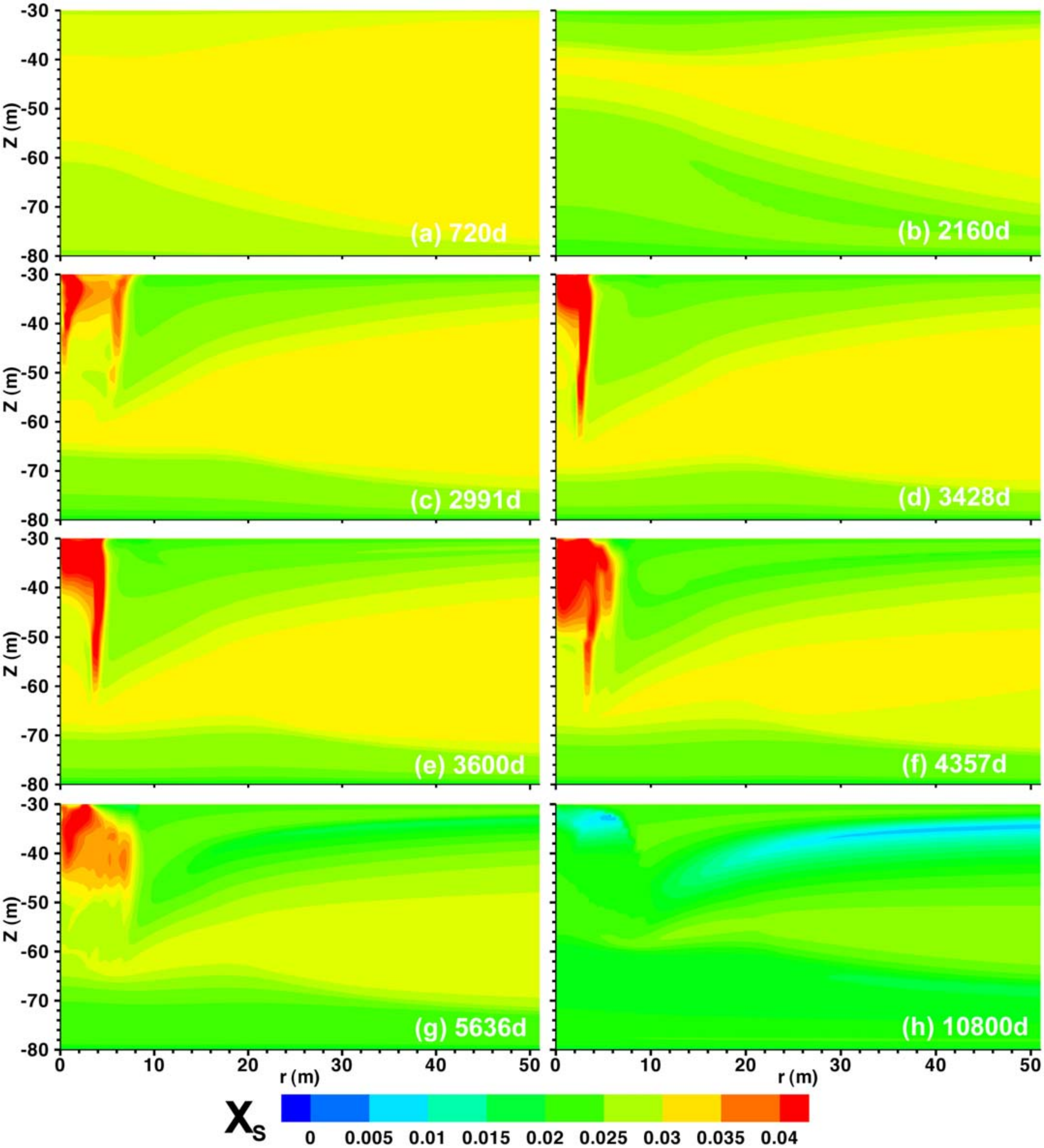

Figure 22 – Evolution of spatial distribution of X_S during gas production from the marine Class 3 hydrate deposit in this study.

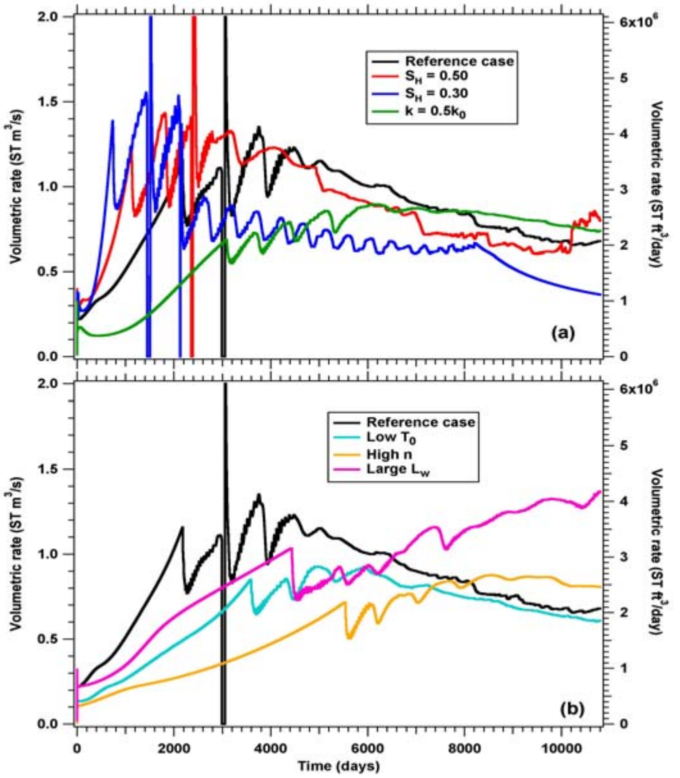

Figure 23 – Sensitivity analysis: effect of various perturbation parameters on the evolution of Q_P during production from the marine Class 3 hydrate deposit in this study.

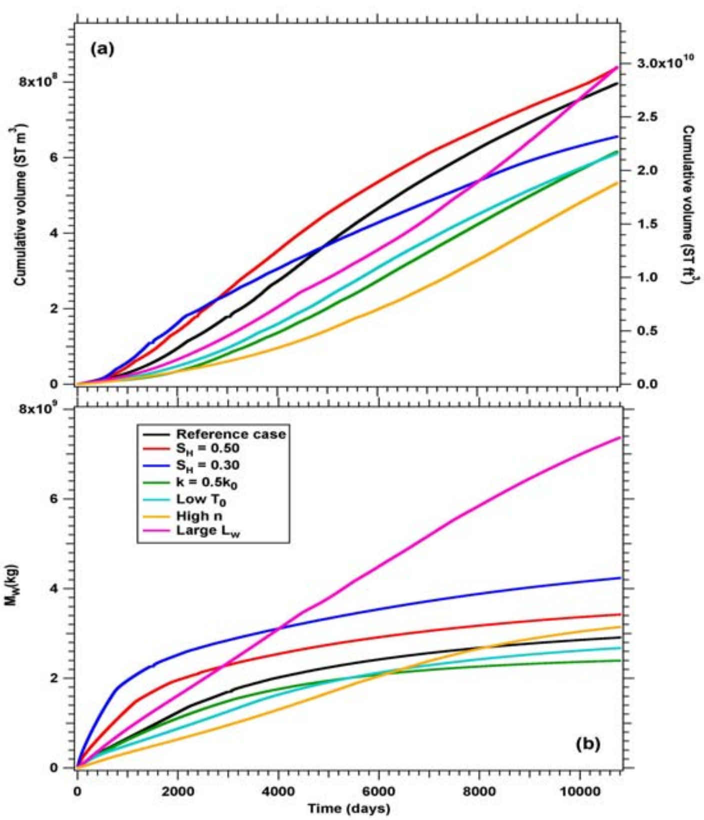

Figure 24 – Sensitivity analysis: effect of various perturbation parameters on the evolution of V_P and M_W during production from the marine Class 3 hydrate deposit in this study.

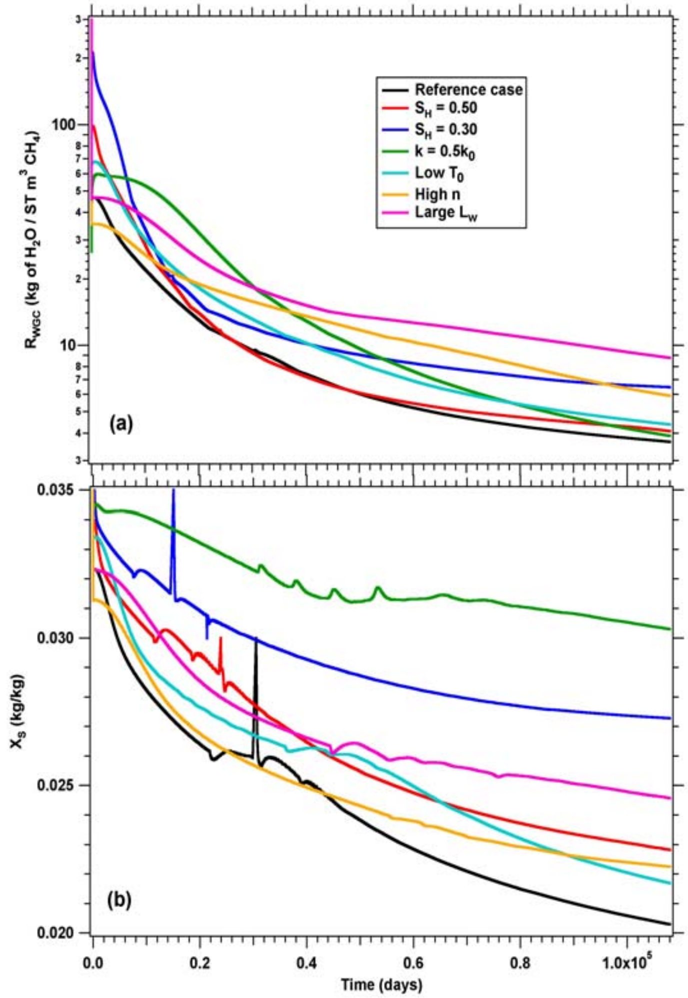

Figure 25 – Sensitivity analysis: effect of various perturbation parameters on the evolution of R_{WGC} and X_P during production from the marine Class 3 hydrate deposit in this study.

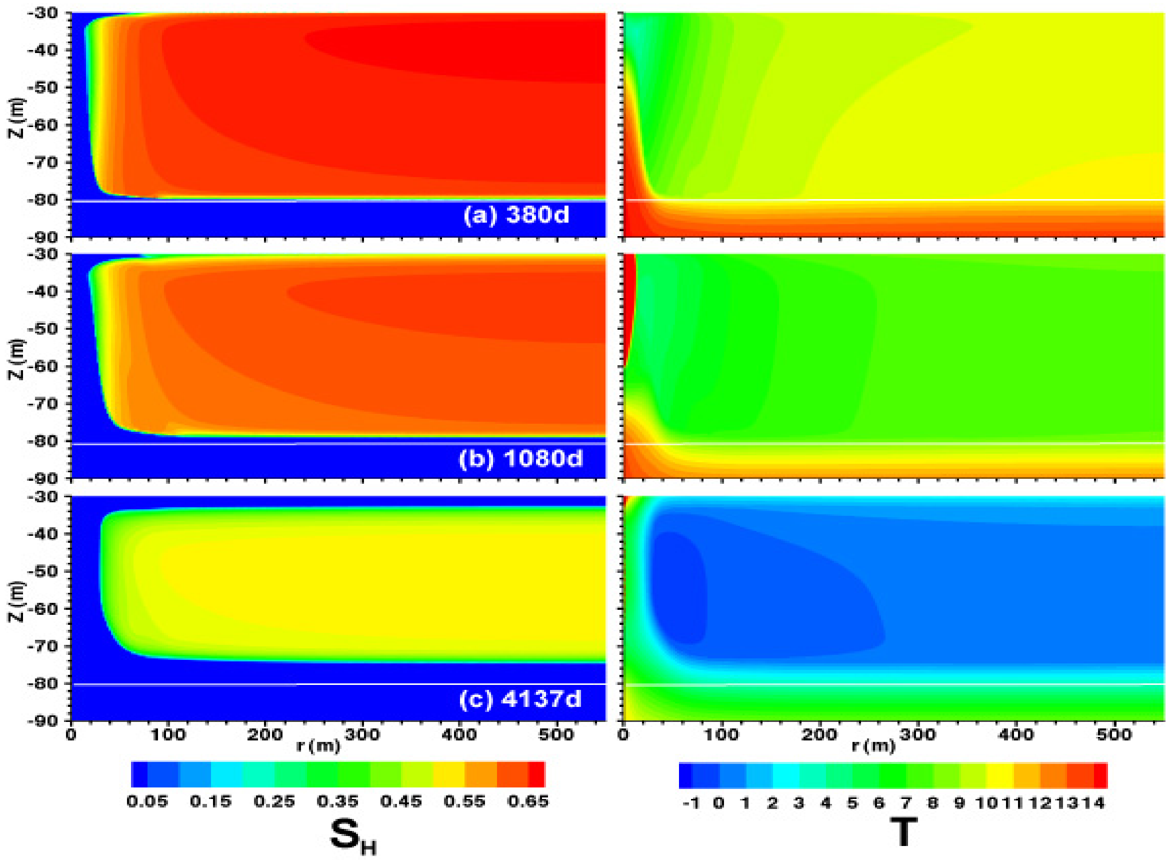

Figure 26 – Uniformity of the S_H and T distributions along r in the marine Class 2 deposit.

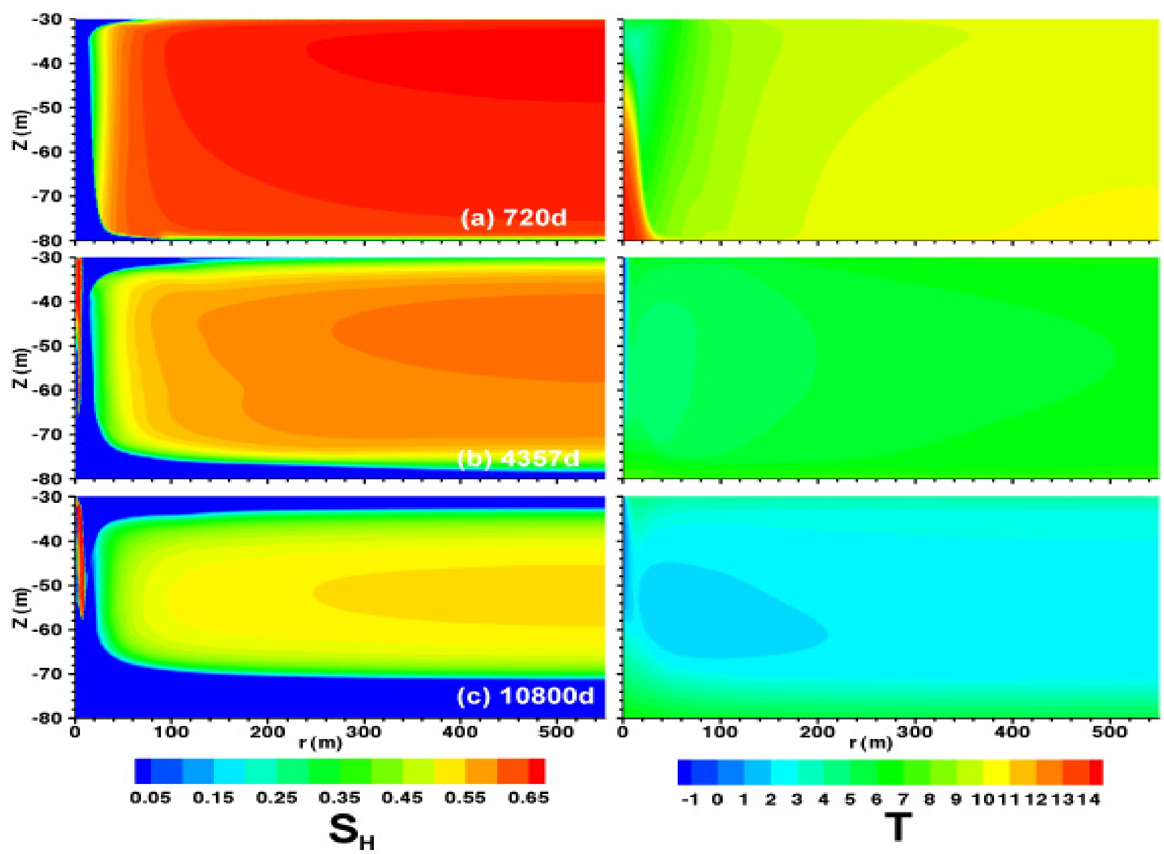

Figure 27 – Uniformity of the S_H and T distributions along r and away from the well in the marine Class 3 deposit.